



HAL
open science

Comparative study on tertiary contacts and folding of RNase P RNAs from a psychrophilic, a mesophilic/radiation-resistant and a thermophilic bacterium

Michal Marszalkowski, Andreas Werner, Ralph Feltens, Dominik Helmecke, Markus Gössringer, Eric Westhof, Roland K Hartmann

► To cite this version:

Michal Marszalkowski, Andreas Werner, Ralph Feltens, Dominik Helmecke, Markus Gössringer, et al.. Comparative study on tertiary contacts and folding of RNase P RNAs from a psychrophilic, a mesophilic/radiation-resistant and a thermophilic bacterium. *RNA*, 2021, pp.rna.078735.121. 10.1261/rna.078735.121 . hal-03328064

HAL Id: hal-03328064

<https://hal.science/hal-03328064>

Submitted on 27 Aug 2021

HAL is a multi-disciplinary open access archive for the deposit and dissemination of scientific research documents, whether they are published or not. The documents may come from teaching and research institutions in France or abroad, or from public or private research centers.

L'archive ouverte pluridisciplinaire **HAL**, est destinée au dépôt et à la diffusion de documents scientifiques de niveau recherche, publiés ou non, émanant des établissements d'enseignement et de recherche français ou étrangers, des laboratoires publics ou privés.

1 **Comparative study on tertiary contacts and folding of RNase P RNAs from a**
2 **psychrophilic, a mesophilic/radiation-resistant and a thermophilic bacterium**

3

4 Michal Marszalkowski^{1,2}, Andreas Werner^{3,4}, Ralph Feltens^{1,5}, Dominik Helmecke¹, Markus
5 Gößringer¹, Eric Westhof³ and Roland K. Hartmann¹

6

7

8 ¹ Philipps-Universität Marburg, Institut für Pharmazeutische Chemie,
9 Marbacher Weg 6, D-35037 Marburg, Germany, e-mail: roland.hartmann@staff.uni-
10 marburg.de

11

12 ² present address: Michał Marszałkowski, ul. Jabłoniowa 22/12, 80-175 Gdańsk, Polska

13

14 ³ Université de Strasbourg, Institut de biologie moléculaire et cellulaire du CNRS,
15 Architecture et Réactivité de l'ARN, 2 allée Konrad Roentgen, F-67084 Strasbourg, France

16

17 ⁴ present address: European Patent Office, Bob-van-Bentham-Platz 1, 80298 Munich,
18 Germany

19

20 ⁵ present address: Berufsschulzentrum 1 der Stadt Leipzig, Crednerstraße 1, D-04289
21 Leipzig, Germany

22

23

24

25 *Running title:* type A RNase P RNA: tertiary contacts and folding

26

27 *Keywords:* interdomain contacts, UV melting profiles, enzyme kinetics, folding, folding
28 trap, thermostability

29 **Abstract**

30

31 In most bacterial type A RNase P RNAs (P RNAs), two major loop-helix tertiary contacts
32 (L8-P4 and L18-P8) help to orient the two independently folding S- and C-domains for
33 concerted recognition of precursor tRNA substrates. Here, we analyze the effects of
34 mutations in these tertiary contacts in P RNAs from three different species: (i) the
35 psychrophilic bacterium *Pseudoalteromonas translucida* (*Ptr*), (ii) the mesophilic
36 radiation-resistant bacterium *Deinococcus radiodurans* (*Dra*), and (iii) the thermophilic
37 bacterium *Thermus thermophilus* (*Tth*). We show by UV melting experiments that
38 simultaneous disruption of these two interdomain contacts has a stabilizing effect on all
39 three P RNAs. This can be inferred from reduced RNA unfolding at lower temperatures
40 and a more concerted unfolding at higher temperatures. Thus, when the two domains
41 tightly interact via the tertiary contacts, one domain facilitates structural transitions in the
42 other. P RNA mutants with disrupted interdomain contacts showed severe kinetic defects
43 that were most pronounced upon simultaneous disruption of the L8-P4 and L18-P8
44 contacts. At 37°C, the mildest effects were observed for the thermostable *Tth* RNA. A
45 third interdomain contact, L9-P1, makes only a minor contribution to P RNA tertiary
46 folding. Furthermore, *D. radiodurans* RNase P RNA forms an additional pseudoknot
47 structure between the P9 and P12 of its S-domain. This interaction was found to be
48 particularly crucial for RNase P holoenzyme activity at near-physiological Mg²⁺
49 concentrations (2 mM). We further analyzed an exceptionally stable folding trap of the
50 G,C-rich *Tth* P RNA.

51 **INTRODUCTION**

52

53 Transfer RNAs (tRNAs) are essential adaptor molecules of cellular protein synthesis
54 machineries. They are synthesized as non-functional precursor transcripts (pre-tRNAs) with
55 flanking sequences at their 5'- and 3'-ends. Ribonuclease P (RNase P) is an essential
56 enzyme that catalyzes the 5'-end maturation of pre-tRNAs (Guerrier-Takada et al., 1983;
57 Waugh and Pace, 1990; Gößringer et al., 2006; Hartmann et al., 2009; Klemm et al., 2016).
58 In the majority of Bacteria, RNase P consists of a catalytically active RNA subunit (P RNA, ~
59 340 to 400 nts) and a small protein subunit (P protein, ~13 kDa) that interacts with
60 nucleotides in the pre-tRNA 5'-leader (Hartmann et al., 2009; Klemm et al., 2016).

61 Bacterial P RNA is a highly structured molecule, with approx. two-thirds of its
62 nucleotides participating in base-pairing interactions. The basic RNA secondary structure,
63 including structural variations, and major tertiary interactions were inferred from
64 phylogenetic/comparative sequence analyses (Brown *et al.*, 1996; Massire *et al.*, 1997 &
65 1998). Deletion studies revealed that only a subset of helices is strictly essential for catalytic
66 function. These helices form the core structure of all bacterial P RNA, while several
67 peripheral helices that are attached to the conserved core structure display a variable
68 occurrence and can be individually deleted with only moderate effects on catalytic function
69 (Waugh et al., 1989; Darr et al., 1992; Haas et al., 1994; Siegel et al., 1996; Schlegl et al.,
70 1994). Based on the different peripheral structural elements, bacterial P RNAs can be
71 classified into two major architectures termed type A (ancestral, *e.g. Escherichia coli*) and
72 type B (Bacillus-like) (Haas et al., 1996; Haas and Brown, 1998; Brown, 1999).

73 RNase P RNA is formed from two independently folding units (Loria & Pan, 1996), the
74 specificity (S-) domain and the catalytic (C-) domain. In bacterial P RNAs of type A
75 architecture, the two functional domains are oriented towards each other with the help of two
76 to three interdomain loop-helix contacts (L18-P8, L8-P4, L9-P1; Fig. 1A-C). Type A RNAs
77 adopt a rather stretched, slightly concave or open umbrella-like overall shape, formed by two
78 layers of helices lying on top of each other. The bound tRNA occupies the position of the

79 umbrella shaft (Reiter et al., 2010; illustrated in Fig. S1). The smaller helical layer consists of
80 the peripheral helices P18 and P13/14 that stabilize the stretched P RNA conformation via
81 their tertiary contacts. The P8/P9 stack is at the interface between the C-domain and the
82 more distal parts of the S-domain (P13/P14 and P7/P10/P11/P12). Structurally, the L8-P4
83 and L1-P9 contacts support the side-by-side arrangement of the P1/P4/P5 and P8/P9 helical
84 stacks (for review, see Gößringer et al., 2021). Among those interdomain contacts, L8-P4 is
85 common and ubiquitous to bacterial P RNAs of type A and B (Massire et al. 1997, 1998). In
86 Archaea, the RNA subunit forms a holoenzyme with five protein subunits (Jarrous and
87 Gopalan, 2010), and folding of the P RNA into its active three-dimensional conformation is
88 more dependent on RNA-protein and protein-protein interactions. This led, for example, to
89 the loss of the L8-P4 interdomain contact in archaeal P RNAs of type M present in
90 *Methanococcales*. Also, the L9-P1 contact, although basically able to form in type M RNAs
91 (Lai et al., 2017), appears to require structural support from interaction of P1/P9 with protein
92 subunits Rpp21/Rpp29 (Wan et al., 2019).

93 The long-range interactions in P RNAs of type A, originally inferred from phylogenetic
94 covariation analyses, were later confirmed in type A P RNA crystal structures as well as in
95 the holoenzyme crystal structure of *Thermotoga maritima* RNase P (Torres-Larios et al.,
96 2005; Reiter et al., 2010). Yet, our knowledge on the individual contributions of these long-
97 range interactions to P RNA function and how they mutually affect folding of the two domains
98 is still incomplete. To address these questions, we have disrupted the L9-P1, L8-P4 and/or
99 L18-P8 interaction by mutation in three model type A P RNAs: the thermostable, G,C-rich P
100 RNA of the thermophile *Thermus thermophilus* (*Tth*), the one from the psychrophilic
101 bacterium *Pseudoalteromonas translucida* (*Ptr*) and the P RNA of *Deinococcus radiodurans*
102 (*Dra*), a mesophilic, radiation-resistant bacterium phylogenetically related to *T. thermophilus*.
103 These three type A P RNAs were chosen because of the following outstanding features. *Tth*
104 P RNA is among the most thermostable P RNAs known. Thermostability of its S-domain was
105 inferred to be achieved by conversion of strategic base pairs to G-C, by decreasing surface
106 accessibility of the native fold and by increasing the amount of structure formation in the

107 native folding transition (Baird et al., 2006). In addition, its two domains form a reinforced L9-
108 P1 contact that contributes to thermostability (Marszalkowski et al., 2008). *Dra* P RNA
109 deviates substantially from canonical type A structures owing to a P9 stem extension, in
110 which L9 has become an internal loop and where the P9 extension forms a pseudoknot (P9c)
111 with L12, likely to reinforce the S-domain structure (Fig. 1B). The P RNA of the psychrophilic
112 bacterium *P. translucida* TAC125 (originally named *Pseudoalteromonas haloplanktis*
113 TAC125; Medigue et al., 2005) may provide hints as to whether adaptation of its host to
114 growth at low temperatures has left traces in the evolution of its P RNA structure. *P.*
115 *translucida* grows at temperatures between 4 and 30°C (Corsaro et al., 2004), *D.*
116 *radiodurans* has an optimal growth temperature of ~ 30°C (Airo et al., 2004; Appukuttan et
117 al., 2006) and *T. thermophilus* grows between 47 and 85°C, optimally thriving at 65 to 72°C
118 (Oshima and Imahori, 1974).

119 To shed light on the role of individual interdomain contacts on P RNA folding and
120 function, we analyzed mutated P RNAs with disrupted interdomain contacts using (i) UV
121 melting to study the effect of the tertiary contacts on RNA folding, (ii) pre-tRNA processing to
122 determine their role for activity and (iii) complementation of a conditionally lethal *E. coli* (*Eco*)
123 P RNA (*mpB*) mutant strain to assess their *in vivo* function in a mesophilic host. We further
124 investigated an exceptionally severe trap in the folding pathway of the thermostable *Tth* P
125 RNA. The RNA was shown to be unable to function in the mesophilic *Eco* host and strictly
126 requires a Mg²⁺-dependent preincubation step at ~55°C for folding *in vitro* into its active
127 structure (Marszalkowski et al., 2008). We thus analyzed this folding trap in more depth via
128 folding kinetics and RNA structure probing.

129

130 RESULTS

131

132 Mutant construction

133 The L18-P8 tertiary contact was disrupted in the three P RNAs (*Tth*, *Dra* and *Ptr*) by mutating
134 the GNRA tetraloop of L18 to an UNCG loop (Fig. 1). Both loops maintain an interaction

135 between positions 1 and 4 of the tetraloop (Pomeranz Krummel and Altman, 1999) to
136 preserve the hairpin-stabilizing ability. The L8-P4 interdomain contact was disrupted by
137 changing the L8 sequence from 5'-AAC to 5'-CGU in the three RNAs (Fig. 1). The UNCG
138 tetraloop mutation was further introduced into L9 of *Tth* (Marszalkowski et al., 2008) and *Ptr*
139 P RNAs to disrupt the L9-P1 contact (Fig. 1A, C). In *Dra* P RNA, the contact between the
140 internal L9 loop and P1 was abolished by changing the bulged A on the 3'-side of L9 to U
141 and by converting the two flanking G•A pairs into G-C pairs (Fig. 1B). For *Dra* P RNA, we
142 also disrupted the idiosyncratic pseudoknot P9c formed between the apical regions of P12
143 and the extended P9 element by mutation of the involved L12 nucleotides (Fig. 1B).
144 Disruption of this intra-S-domain interaction enabled us to assess to which extent this
145 interaction contributes to RNA folding and function.

146

147 **UV melting studies**

148 Folding of P RNA proceeds from an unfolded (U) state, traverses a counterion-dependent
149 intermediate state (I) to reach the final Mg^{2+} -dependent native (N) state. In the I state, the
150 majority of base-pairing and stacking interactions have formed. The transition of the P RNA
151 structure from the I to the U state (and vice versa) can be measured by UV spectroscopy.
152 However, near-UV circular dichroism (CD) is required to study the second transition (I to N)
153 that mainly changes the molecular compactness and helicity parameters (Pan and Sosnick,
154 1997). Mg^{2+} ions not only contribute to charge shielding, but also occupy specific Mg^{2+}
155 binding sites. In addition, Mg^{2+} ions can stabilize kinetic folding traps. As this complicates UV
156 melting profiles, we performed melting experiments in the presence of 100 mM Na^+ and
157 absence of Mg^{2+} to confine the effects of counterions to electrostatic shielding. We also
158 noticed that folding in the presence of Na^+ was always more reproducible than with Mg^{2+} ,
159 associated with the additional advantage that the RNA could be subjected to repeated
160 heating and annealing cycles while avoiding the risk of metal ion-induced P RNA degradation
161 at high temperatures.

162 The first derivative dA_{260}/dT curves of the three wildtype (WT) P RNAs (green curves
163 in Fig. 2, profiles on the right) revealed major melting transitions at $\sim 60^\circ\text{C}$ for *Ptr* P RNA, at
164 $\sim 57^\circ\text{C}$ and $\sim 74^\circ\text{C}$ for *Dra* P RNA and at $\sim 75^\circ\text{C}$ for *Tth* P RNA (Figs. 2A-C). A substantial
165 contribution to the 74°C transition of the *Dra* P RNA may originate from the long G,C-rich
166 P8/P9/P9b/P9c stack (Fig. 1B).

167 The effects of mL8 and mL18 mutations (disrupting the L8-P4 and L18-P8
168 interdomain contacts, respectively) on UV melting profiles depended on the type of P RNA.
169 Both mutations individually had a destabilizing effect on *Ptr* P RNA, where they caused some
170 partial structures to melt at lower temperatures (approx. between 20 to 40°C) than in the WT
171 P RNA. The melting profile of *Tth* P RNA was only marginally affected by either the mL8 or
172 mL18 mutation, while both mutations individually stabilized the *Dra* P RNA, as inferred from
173 the observed reduced unfolding between 50 to 57°C (Fig. 2B, profiles on the right).
174 Particularly the mL18 mutation changed the *Dra* P RNA melting profile to a major peak at
175 $\sim 64^\circ\text{C}$ in the first derivative curve. However, simultaneous disruption of both interdomain
176 contacts, L18-P8 and L8-P4, stabilized all three P RNAs, in the sense that more structure
177 unfolded concertedly at higher temperatures (Fig. 2, profiles on the right). For *Ptr* P RNA, this
178 went along with an upshift of the major peak to $\sim 62^\circ\text{C}$ (mL8/L18) and markedly decreased
179 hyperchromicity at lower temperatures (Fig. 2A). For *Dra* and *Tth* P RNA, the double
180 mutation decreased melting of structures in the temperature range of $\sim 40^\circ\text{C}$ (*Dra*) or $\sim 30^\circ\text{C}$
181 (*Tth*) to almost 60°C (Figs. 2B, C). Overall, the stabilizing effect upon disrupting the L18-P8
182 and L8-P4 interdomain contact was most pronounced for *Ptr* P RNA, the most A, U-rich of
183 the three compared RNAs.

184 Measurements with the isolated *Ptr* S-domain revealed that the major unfolding
185 transition of the WT *Ptr* P RNA ($\sim 59^\circ\text{C}$) is split into two peaks at 62°C and 72°C , respectively
186 (Fig. 3B). Thus, the *Ptr* S-domain is more stable than the full-length WT P RNA, and its major
187 transition at 62°C coincides with that of the full-length P RNA carrying the mL8/L18 double
188 mutation (Fig. 3B, right panel). The effects of long-range interactions on the UV melting
189 profile are not confined to interdomain contacts. Disruption of the intra-S-domain L12-L9c

190 pseudoknot in the P9c mutant had a similar effect as the mL18 mutation in the context of the
191 full-length *Dra* P RNA, resulting in a more concerted and upshifted melting transition at 62°C
192 (Fig. 4, 2B, right panels). Restoring pseudoknot formation by introducing compensatory
193 mutations into the P9c mutant again reduced the prevalence of the transition at ~62°C similar
194 to the WT *Dra* P RNA (Fig. 4).

195

196 **A folding trap of *T. thermophilus* RNase P RNA**

197

198 *In vitro* transcripts of *T. thermophilus* P RNA require a preincubation step at temperatures
199 higher than 37°C (e.g. at 55°C) for activation (Hartmann and Erdmann, 1991; Marszalkowski
200 *et al.*, 2008). This suggested that the native folding transition has an extraordinarily high
201 activation energy barrier so far unprecedented among bacterial P RNAs. Here we analyzed
202 the nature of this temperature-dependent folding transition in more detail. The requirement
203 for a 55°C preincubation step was seen at Mg²⁺ concentrations between 10 to 100 mM Mg²⁺
204 (Supplemental Fig. S2A). In contrast, preincubation of *Eco* P RNA at 55°C versus 37°C had
205 no or at most a twofold effect, depending on the Mg²⁺ concentration (Supplemental Fig.
206 S2B). Folding kinetics of *Tth* P RNA were further investigated at 20 nM P RNA and 200 nM
207 pre-tRNA in the RNA-alone reaction in the presence of 20 mM Mg²⁺. Preincubation of *T.*
208 *thermophilus* P RNA for 15 min at 37°C instead of 55°C resulted in slow substrate turnover
209 and sigmoidal kinetics (Fig. 5, curve a versus b). When the RNA was preincubated for 5 h at
210 37°C before pre-tRNA addition, the rate of substrate cleavage increased, but still did not
211 reach that obtained after preincubation for 15 min at 55°C (Fig. 6, curve c versus b). We also
212 analyzed if the presence of the substrate may assist (or inhibit [Pan and Sosnick, 1997]) *T.*
213 *thermophilus* P RNA folding into an active conformation. After P RNA preincubation for 15
214 min at 37°, addition of substrate and incubation for 285 min (without withdrawal of aliquots),
215 fresh ptRNA substrate (200 nM) was added and the reaction monitored for another 285 min
216 by withdrawal of aliquots and analysis by 20% denaturing PAGE. The resulting curve d (Fig.
217 6) was almost identical to curve c (P RNA preincubated for 5 h min at 37°C), suggesting that

218 the presence of substrate had little effect on the slow refolding kinetics at 37°C and 20 mM
 219 Mg²⁺. The sigmoidal curve "a" could be fitted to equation 1 (see below), with k_{obs} describing
 220 the pseudo-first order rate constant when essentially all P RNAs are folded (as assumed to
 221 be accomplished by preincubation for 15 min at 55°C), k_1 the first order rate constant for the
 222 slow folding step at 37°C, c the concentration of substrate at any time point, and c_0 the
 223 concentration of substrate at the start of the reaction.

224

225 Equation 1:

$$226 \frac{C}{C_0} = \text{Limit} \cdot \left(1 - e^{-k_{\text{obs}} \times t} \cdot e^{\frac{k_{\text{obs}} \times e^{-k_1 \times t_0}}{k_1} (1 - e^{-k_1 \times t})} \right)$$

227

228 If the rate of cleavage after preincubation at 55°C (Fig. 5, curve b, $k_{\text{obs}} = 0.083 \text{ min}^{-1}$) is
 229 taken as k_{obs} in equation 1, a k_1 value of 0.0016 min^{-1} for the folding step at 37°C is
 230 calculated. The overall folding rate of *Eco* P RNA was determined as 0.54 min^{-1} (Kent et al.,
 231 2000), thus being more than 300-fold faster under similar conditions (25 mM Mg²⁺, 120 mM
 232 KCl, pH 7.0, 37°C). We further measured the rate of folding to the native state via processing
 233 activity assay as a function of *Tth* P RNA preincubation time at 55°C. The folding rate was
 234 determined as 0.13 min^{-1} (Supplemental Fig. S3A). When P RNA preincubation was
 235 performed at 3 M urea, a folding rate enhancement of up to fourfold was observed
 236 (Supplemental Fig. S3B), indicating the presence of one or more kinetic traps along the
 237 folding pathway (Pan and Sosnick, 1997).

238 A preincubation step at 55°C for P RNA activation was also required in the
 239 holoenzyme reaction and efficient P RNA folding depended on the presence of Mg²⁺ (4.5
 240 mM) during this step (Supplemental Fig. S4A,B). We also analyzed the effect of the
 241 preincubation step performed at 37°C versus 55°C on RNA alone activity for the *Tth* mL8,
 242 mL9, mL18 and mL8/L18 mutant P RNAs (Supplemental Fig. S4C). As for the WT *Tth* P
 243 RNA, substantial activity was only obtained upon P RNA preincubation at 55°C.

244

245 **Analysis of *T. thermophilus* P RNA folding by RNase T1 probing**

246

247 The structure of *Tth* P RNA was probed by RNase T1 digestion under non-denaturing
248 conditions (Fig. 6). RNase T1 cleaves 3' of exposed G residues in flexible regions, and it was
249 already shown for the *Tth* S-domain that accessibility of G residues largely decreases from
250 the I to the N state (Baird et al., 2006). For RNase T1 probing, 5'- or 3'-end-labeled P RNA
251 was preincubated at 37°C or 55°C, followed by probing at 37°C. The following regions
252 became protected from RNase T1 cleavage upon preincubation of 5'-end-labeled *Tth* P RNA
253 at 55°C versus 37°C (Fig. 6A, gray vertical lines on the right): P11 (3'-strand), L13 (G192),
254 J11/12, P10, P9, P6-8, P4, J3/4, and the 3'-side of P3. 3'-end-labeled *Tth* P RNA provided
255 partially overlapping information, such as protection at G226/7 or signal enhancement (filled
256 dots) at G252/3 upon preincubation at 55°C; signal intensities were also increased for
257 cleavages in the 3'-part of L15 and in J17/16 (Fig. 6C).

258 We also analyzed the *Tth* mL9 mutant RNA (Fig. 1C) by RNase T1 probing as a
259 function of preincubation temperature. The pattern of protection from RNase T1 hydrolysis
260 upon preincubation at 55°C was very similar to that obtained with the WT RNA (Fig. 6B vs.
261 A). The protection of J3/4 upon preincubation at 55°C was less pronounced than for the *Tth*
262 WT P RNA, suggesting that formation of the L9-P1 contact buries more tightly those residues
263 in the catalytic core. This minor difference compared with the WT P RNA is consistent with
264 the moderate activity decrease of the mL9 variant in the RNA-alone reaction at high
265 temperatures (55°C) and at low Mg²⁺ concentrations in the holoenzyme reaction
266 (Marszalkowski et al., 2008).

267 In summary, RNase T1 probing revealed substantial structural compaction and
268 surface burial in the S-domain upon preincubation at 55°C, particularly in P6-9, P11 and
269 J11/12. Similar protections from RNase T1 cleavage were observed with the isolated *Tth* S-
270 domain upon increasing the Mg²⁺ concentration from 0.05 to 1.6 mM, conditions that were
271 considered to represent the intermediate (I) and native (N) fold of the S-domain, respectively

272 (Baird et al., 2006). The overlap between these previous results and our findings suggests
273 that the folding state of the S-domain within the full-length RNA and before preincubation at
274 55°C resembles the I state of the isolated S-domain in the study by Baird et al. (2006).

275 In the C-domain, major compaction occurred in the P6 region (Fig. 6A), suggesting
276 that this structural element forms during the 55°C temperature step. Another area of
277 compaction is the 3'-side of P3, J3/4 and helix P4 near its U bulge in the catalytic core. In
278 addition, RNase T1 accessibility in the P15-17 region changed from the I to the N state.

279

280 **Enzyme kinetic effects upon disruption of L8-P4 and/or L18-P8 interdomain contacts**

281

282 The functional role of interdomain contacts in *Ptr*, *Tth* and *Dra* P RNAs was analyzed in
283 single turnover kinetic RNA-alone reactions at 37°C (Table 1). Disruption of the L8-P4
284 contact had little effect on *Tth* P RNA (1.4-fold decrease in $k_{\text{react}}/K_{\text{m(sto)}}$ relative to the WT
285 RNA) but affected *Ptr* and *Dra* P RNAs more severely (37- and 92-fold decrease in
286 $k_{\text{react}}/K_{\text{m(sto)}}$; Table 1). A similar trend was observed for P RNA variants with a disrupted L18-
287 P8 interaction (approx. 6-, 37- and 28-fold decrease in $k_{\text{react}}/K_{\text{m(sto)}}$ for *Tth*, *Ptr* and *Dra* P RNA,
288 respectively; Table 1). For *Tth* P RNA, the kinetic defect upon disruption of the L18-P8
289 interaction was more pronounced in cleavage assays performed at 55°C (under otherwise
290 similar conditions; Schlegl et al., 1994) instead of the 37°C uniformly applied in the present
291 study.

292 Simultaneous disruption of the L8-P4 and L18-P8 contacts (variants mL8/L18)
293 impaired activity more severely. Catalytic efficiency ($k_{\text{react}}/K_{\text{m(sto)}}$) for the *Tth* mL8/L18 variant
294 was now ~22-fold decreased and ~430-fold and ~3000-fold for the *Ptr* and *Dra* mL8/L18
295 variants, respectively (Table 1). Surprisingly, simultaneous disruption of the two interdomain
296 contacts was most detrimental to *Dra* P RNA function. This may be related to the extension
297 of the P8-P9 stem that is further constrained by the P9c pseudoknot in *Dra* P RNA. In the
298 absence of the L8-P4 and L18-P8 tertiary contacts, the extended and rigidified P8-P9 stem
299 may be difficult to keep in a productive orientation toward the C-domain or may even lead to
300 steric clashes with the substrate. As a general trend, the thermostable *Tth* P RNA structure

301 turned out to be more robust than P RNAs from *Ptr* and *Dra*, as inferred from the lower
302 sensitivity of the former RNA toward loss of individual interdomain contacts under the
303 conditions tested, in line with previous findings (Marszalkowski et al., 2008). Overall, these
304 findings are consistent with a basic assumption of our model presented in Fig. 7, namely that
305 one functional interdomain contact, L8-P4 or L18-P8, can principally maintain domain
306 orientation, while the absence of both contacts severely depletes the fraction of P RNA
307 molecules with a productive domain arrangement.

308

309 **Analysis of the L9-P1 interaction in *Ptr* and *Dra* P RNAs**

310

311 We extended our studies to the L9-P1 contact in *Ptr* P RNA. P9 of this RNA harbors a 5'-
312 GCGA-3' tetraloop that is predicted to dock onto the second and third bp in P1. For cloning
313 and expression purposes we changed the second P1 bp of *Ptr* P RNA from A:U to G:C (Fig.
314 1A). We considered it unlikely that this bp exchange would substantially weaken the L9-P1
315 interaction (see Fig. S6 and its discussion in the Supplement). For the *Ptr* mL9 mutant RNA,
316 we neither saw a defect in the RNA-alone reaction at 37°C (Table 1) nor in the holoenzyme
317 reaction with the heterologous *E. coli* or *B. subtilis* P protein (Table 2). This suggested that
318 the P1-L9 interaction does not make a substantial contribution to the overall stabilization of
319 *Ptr* P RNA at 37°C, in line with the corresponding findings for *Eco* P RNA (Pomeranz
320 Krummel and Altman, 1999; Marszalkowski et al., 2008). A possible explanation is that the
321 L9-P1 contact forms only concomitantly (opportunistically) when the L8-P4 and L18-P8
322 contacts are in place, but in this native context disruption of the L9-P1 contact remains
323 phenotypically silent. To clarify whether the L9-P1 contact can yet form independently, we
324 compared the kinetic performance of *Ptr* mL8/L18 double and *Ptr* mL8/L18/L9 triple mutants.
325 In both mutants, we also restored the native A2:U360 bp in P1 to entirely exclude any effect
326 of the G2:C360 bp exchange on the L9-P1 interaction. Single turnover RNA-alone kinetics
327 under our standard conditions (see Table 1) revealed no significant difference between the
328 *Ptr* mL8/L18 P RNA used in Table 1 (with bp G2:C360) relative to the *Ptr* mL8/L18 P RNA

329 with the native A2:U360 bp. However, the *Ptr* mL8/L18/L9 P RNA triple mutant (with bp
330 A2:U360) showed a twofold increase in $K_{m(sto)}$ and a twofold decrease in k_{react} (based on ≥ 11
331 individual kinetic experiments conducted in parallel for each of the three P RNAs). These
332 findings indicate that the L9-P1 contact can form independently in *Ptr* P RNA, but its
333 contribution to stabilizing the active fold at 37°C is minor.

334 We further analyzed activity of the *Dra* mL9 and mP9c mutant P RNAs. The *Dra* mL9
335 mutant P RNA showed a minor (1.4-fold) reduction of catalytic efficiency in RNA-alone
336 assays performed at 37°C (Table 1). Likewise, holoenzymes assembled from the *Dra* mL9 P
337 RNA showed essentially no difference compared with holoenzymes containing the WT P
338 RNA when assayed at 4.5 mM Mg²⁺, and only moderately reduced cleavage rates at 2 mM
339 Mg²⁺ (1.5-fold with *E. coli* RnpA and 6.4-fold with *B. subtilis* RnpA; Table 2). This suggests
340 that the L9-P1 contact forms in this P RNA but makes only a minor contribution to
341 interdomain orientation, as observed for *Ptr* P RNA. In contrast, much more severe defects
342 were observed for the *Dra* mP9c mutant RNA particularly in holoenzyme reactions performed
343 at 2 or 4.5 mM Mg²⁺ (activity losses of 3 to 4 orders of magnitude; Table 2).

344

345 ***In vivo* complementation analysis**

346

347 The WT and mutant P RNAs were tested for their capacity to rescue the lethal phenotype of
348 the *Eco* P RNA (*rnpB*) mutant strain BW (Wegscheid and Hartmann, 2006). Among the
349 heterologous *rnpB* genes, only that of *Ptr* was able to rescue growth of the mutant strain
350 when provided on a low copy plasmid (Table 2). The failure of *Tth* *rnpB* genes
351 (Marszalkowski et al., 2008) to functionally replace *Eco* *rnpB* can be explained by the fact
352 that this RNA of thermophilic origin requires temperatures $\gg 37^\circ\text{C}$ (e.g. 55°C) for efficient
353 folding (see above), suggesting insufficient folding in the *E. coli* host cultivated at 37° or
354 43°C. For *Dra* P RNA, the failure may be related to its unique architecture in the P9 and P12
355 regions (Fig. 1), possibly entailing idiosyncratic requirements for the folding process *in vivo*.
356 This might also be related to expression of a non-canonical P protein in *D. radiodurans* that

357 is predicted to carry a C-terminal extension according to genome annotations. Hence, we
358 could only test the *Ptr* mutant P RNAs for complementation in strain BW. Whereas the mL8
359 and mL8/L18 variants were non-functional, a partial rescue of the growth phenotype was
360 seen for the mL18 variant (Table 2). This suggests that, *in vivo*, the L8-P4 contact is more
361 crucial for P RNA function than the L18-P8 interaction, which is consistent with its presence
362 in both types A and B P RNAs and the observation that the P18 element has been lost in P
363 RNAs of some bacterial clades, such as in the *Aquificales* and the genus *Chlorobium*
364 (Marszalkowski et al., 2006; Haas et al. 1994).

365 Full rescue of growth of *E. coli* strain BW under non-permissive conditions was
366 observed upon expression of the *Ptr* mL9 mutant P RNA (Table 3). Remarkably,
367 complementation in *E. coli* was also successful at 43°C, thus substantially above the
368 maximum growth temperature (30°C) of *P. translucida*. The finding supports the notion that
369 the L9-P1 interaction is of low relevance for function of *Ptr* RNase P if the L8-P4 and L18-P8
370 interactions are in place.

371

372 DISCUSSION

373

374 The present UV melting analyses have revealed that formation of the L8-P4 and L18-P8
375 contacts affect structural transitions in one or both P RNA folding domains. Disabling one of
376 the two tertiary contacts has a destabilizing effect in the context of *Ptr* P RNA, a stabilizing
377 effect on *Dra* P RNA and a marginal effect on *Tth* P RNA. Such differential effects on melting
378 profiles of *Ptr* versus *Dra* P RNA may be related to some A,U-rich, low stability structural
379 elements in the *Ptr* P RNA (such as P8 or P18; Fig 1A) that are stabilized in the native fold.
380 Yet, these partly opposing effects occurred in a context where one of the major interdomain
381 struts (L8-P4 or L18-P8) is assumed to keep a substantial fraction of molecules in the
382 functional interdomain orientation (see below). However, upon simultaneous disruption of
383 both interdomain contacts (mL8/L18 double mutant), interactions between the C- and S-
384 domains are largely lost. The L9-P1 contact is too weak to compensate for the combined

385 disruption of the L18-P8 and L8-P4 contacts. As a result, a uniform overall effect was
386 observed for all three P RNAs: C- and/or S-domains were stabilized such that melting
387 occurred more concertedly with less unfolding at lower temperatures. The net stabilizing
388 effects seen in the melting profiles of the double mutants may have masked minor
389 destabilizing effects, such as those seen for *Ptr* P RNA upon disruption of the L18-P8 or L8-
390 P4 contact. Since the folding processes are reversible in denaturation and renaturation UV
391 spectroscopy experiments (Fig. S6), we conclude that one domain acts as an *unfolding*
392 *chaperone* of the other. When the two domains tightly interact, each domain lowers the
393 inherent stability of the other domain (see model in Fig. 7). This may be due to exchange of
394 interactions from intra- to inter-domain contacts, especially, but not solely, at the interaction
395 interface (L18-P8 and L8-P4). More indirect effects are conceivable as well, for example that
396 the tertiary interactions induce deviations in coaxial stackings between helices that are part
397 of helical stacks in P RNA.

398 In line with the UV melting results, the mL8/L18 double mutation showed the most
399 severe catalytic defect for all three P RNAs, supporting the above assumption that the
400 fraction of P RNA molecules that adopt a productive interdomain orientation is largely
401 decreased in the absence of the L8-P4 and L18-P8 contacts. This depletes the pool of
402 catalytic RNA molecules that are able to position the pre-tRNA substrate for concerted
403 recognition of the tRNA D/T loop by the S-domain and docking of the cleavage site to the
404 active site in the C-domain. The single mL8 and mL18 mutations caused less severe
405 catalytic defects, in line with smaller changes in the UV melting profiles relative to the
406 mL8/L18-double mutant. This supports the notion that maintaining one of the two tertiary
407 contacts still allows a substantial fraction of P RNAs to adopt a productive interdomain
408 orientation. The thermostable *Tth* P RNA showed the lowest activity decreases upon
409 disruption of the L8-P4, L18-P8 or both contacts. One reason could be its strengthened L9-
410 P1 contact (see below) combined with its reduced conformational flexibility at 37°C, which is
411 well below the growth temperature range of *T. thermophilus* (~50 and 85°C). This may have
412 increased the fraction of mutant P RNAs that adopt an active fold relative to P RNAs of

413 mesophilic or psychropilic origin.

414 While we stressed the role of the L18-P8 contact for domain orientation, some
415 previously reported functional and structural consequences of its disruption are noteworthy.
416 For *Eco* P RNA, deletion of P18 caused a substrate binding (K_m) defect *in vitro* at 25 mM
417 Mg^{2+} and 1 M NH_4^+ . This defect could be rescued by increasing the NH_4^+ concentration to 3
418 M (Haas et al., 1994). Likewise, enzyme activity of *Eco* P RNA with a mutated L18 loop (5'-
419 UUCG) could be largely rescued by elevating the Mg^{2+} concentration to 190 mM at 100 mM
420 NH_4^+ (Pomeranz Krummel and Altman, 1999). This suggested electrostatic repulsion effects
421 between enzyme and substrate RNAs upon disruption of the L18-P8 contact. Kirsebom and
422 coworkers probed *Eco* WT and mL18 (5'-CUUG) P RNA with Pb^{2+} ions and RNase T1 (Mao
423 et al., 2018). They observed structural changes in P11 and at the junction between P14 and
424 P11 in the S-domain of the mL18 mutant RNA with disrupted L18-P8 interaction. In addition,
425 there was a change in RNase T1 susceptibility at helix P5 in the C-domain, close to the
426 active site. Generally, higher Pb^{2+} concentrations were required for the mL18 versus WT P
427 RNA to induce backbone hydrolysis at high affinity metal ion binding sites (Mao et al., 2018).
428 This can be explained by a more flexible structure of the mutant RNA, resulting in affinity
429 losses at Mg^{2+} binding sites. Even charge distribution at the substrate cleavage site was
430 found to be affected by disruption of the L18-P8 interaction. This was analyzed with a
431 substrate carrying a protonable 2'- NH_2 group at nt -1 near the canonical cleavage site. The
432 mL18 mutation caused changes in the fraction of substrate that was cleaved at the canonical
433 cleavage (-1/+1) site at different pH values (Mao et al., 2018). The authors proposed that the
434 L18-P8 interaction acts as structural mediator between the substrate (T stem-loop) binding
435 region in the S-domain and the active center of the C-domain. The contact supports the
436 binding of structurally and catalytically relevant Mg^{2+} ions, supports native P RNA folding
437 particularly in the S-domain and optimizes positioning of chemical groups and catalytic Mg^{2+}
438 ion during catalysis. Noteworthy, *Eco* WT and mL18 P RNA were also analyzed by UV
439 melting in a buffer containing 0.4 M NH_4^+ and 1 mM Mg^{2+} (Pomeranz Krummel and Altman,

440 1999). The mL18 mutation had a destabilizing effect on *Eco* P RNA, as we observed for *Ptr*
441 P RNA (Fig. 2A), underscoring the resemblance of the two bacterial type A RNAs.

442 Certain thermophilic bacteria, such as *T. thermophilus*, have a 5'-GYAA L9 tetraloop
443 and a P1 receptor site consisting of a G-C bp tandem (Massire et al., 1997, Marszalkowski et
444 al., 2006). Such tandem type I/II G-C:A nucleoside triples, where the consecutive A residues
445 interact with the entire (type I) or half (type II) minor groove of the respective G-C bp,
446 represent the most stable combination for this kind of tertiary contact (Doherty et al., 2001).
447 The L9-P1 interdomain contact was shown to contribute to activity of *Tth* P RNA at elevated
448 temperatures and physiological Mg^{2+} concentrations. Its disruption by L9 loop mutation
449 prevented formation of a compact conformer observed in native PAA gels (Marszalkowski et
450 al., 2008). In contrast, L9 mutations in *Eco* P RNA, where two A residues are predicted to
451 interact with a G-U and A-U bp (Massire et al., 1997), had no or little effect on function *in*
452 *vitro* and *in vivo* (Pomeranz Krummel and Altman, 1999; Marszalkowski et al., 2008).
453 Likewise, we demonstrated here that a loss of the L9-P1 contact in *Ptr* P RNA does not
454 abrogate the ability to replace the native *Eco* P RNA *in vivo*. Consistent with this finding, the
455 *Dra* mL9 P RNA showed only a minor reduction in catalytic efficiency *in vitro*. By testing the
456 mL9 mutation in *Ptr* P RNA in the context of disrupted L18-P8 and L8-P4 contacts, we were
457 able to carve out that the L9-P1 contact can form independently. However, its functional
458 contribution was found to be minor. This supports the notion that contacts L8-P4 and L18-P8
459 are most important for maintaining the functional interdomain orientation in bacterial P RNAs
460 of type A. The enhanced functional role of the L9-P1 contact in thermostable P RNAs with a
461 5'-GYAA L9 and a tandem G-C bp receptor in P1 may also include contributions from the
462 more rigid structural context of the contact. This includes the G-C bp tandem in P1 and the
463 general stabilization of helices, including P1 and P9, by helix extension and/or deletion of
464 nucleotide bulges (Marszalkowski, et al., 2006; Baird et al., 2006). This implies that the L9-
465 P1 contact might form more stably in *Ptr* P RNA at physiological temperatures of its host
466 bacterium (4 to 30°C) owing to reduced conformational dynamics of the RNA relative to
467 37°C.

468 The disruption of the idiosyncratic P9c pseudoknot contact in *Dra* P RNA moderately
469 affected catalytic performance (~7-fold) in the RNA-alone reaction at high Mg^{2+}
470 concentration (100 mM; Table 1). However, the mP9c mutation drastically reduced
471 holoenzyme activity at low Mg^{2+} (~ 10^3 -fold at 4.5 mM Mg^{2+} , Table 2). Reducing the Mg^{2+}
472 concentration from 4.5 to 2 mM further reduced holoenzyme activity ($\leq 10^4$ -fold), indicating
473 that P9c pseudoknot formation is particularly crucial in the holoenzyme context at
474 physiological Mg^{2+} concentrations.

475 Although the psychrophilic bacterium *P. translucida* grows in the range of 4 to 30°C,
476 its P RNA can functionally replace *Eco* P RNA *in vivo* at temperatures above this
477 temperature range (37° or 43°C, Table 2); likewise, the *Ptr* P protein was fully functional in *B.*
478 *subtilis* at 37°C (Gößringer and Hartmann, 2007), showing that *Ptr* RNase P components are
479 stable at temperatures above the growth temperature limit of the bacterium (30°C). This may
480 suggest that bacterial P RNA ribozymes require a certain minimum overall stability, *i.e.* a
481 minimum number of G-C base pairs, to fold into their functional architecture without the help
482 of protein cofactors. Examples of more A/U-rich P RNAs are only found in eukaryotic
483 organelles, where these RNAs depend on multiple protein cofactors for folding and activity
484 (Schencking et al., 2020). Nevertheless, the *Ptr* P RNA has a reduced G,C content (~54%)
485 relative to the mesophilic *Eco* P RNA (~62%), suggesting increased structural flexibility of the
486 P RNA as an adaptation to psychrophilic growth, in line with the pronounced changes in UV
487 spectra upon introducing the mL8 and/or mL18 mutation(s) (Fig. 2A). Indeed, several helical
488 elements in *Ptr* P RNA show hallmarks of reduced stability/increased flexibility (increases in
489 A-U and non-Watson-Crick base pairs, additional bulges; see P1, P3, P8, P18, P11, P12,
490 P17 in Fig. 1A). In this context, we compared the pre-tRNA processing kinetics at assay
491 temperatures of 37°C versus 15°C (Supplemental Tables 1 and 2). The cleavage rate
492 constant k_{react} at 15°C was indeed the highest for *Ptr* P RNA (compared with *Eco*, *Dra* and
493 *Tth* P RNAs) in the RNA-alone reaction (Supplemental Table 1), possible reflecting an
494 adaptation to activity at low temperatures. However, this should be interpreted with caution,
495 because we only measured the processing reaction itself at 15°C, while RNA folding and

496 holoenzyme assembly were conducted at 55/37°C. Thus, these experiments did not address
497 effects of low temperature on P RNA and tRNA folding as well as holoenzyme assembly;
498 furthermore, the assembly of the *Ptr* holoenzyme was performed with the *Eco* P protein
499 (Supplemental Table 2).

500 While *D. radiodurans* R1 optimally grows at ~30°C, its P RNA has characteristics of a
501 thermostable RNA: its G+C content is ~69% (71.4% in *Tth* P RNA) and its processing activity
502 peaks at ~50°C (that of *Tth* P RNA at ~60°C; measured at 25 mM MgCl₂ and 1 M NH₄Cl).
503 This might contribute to the versatile resistance of the bacterium to stresses including
504 gamma and UV radiation (Aira et al., 2004; Battista, 1997; Setlow and Boling, 1965), as
505 backbone breaks in thermostable RNAs are less detrimental to RNA function than in
506 mesophilic RNAs. For example, *in vitro* activity losses of the thermostable *Tth* P RNA upon
507 Pb²⁺-induced fragmentation were less pronounced than for *Eco* P RNA (Ciesiolka et al.,
508 1994).

509 The group I self-splicing intron is an example of an RNA that first and rapidly folds
510 into a nucleating core structure (the P4/P6 domain), which then serves as a scaffold for
511 folding of its second domain (Doherty and Doudna, 1997). In contrast, the two domains of
512 bacterial P RNAs (S- and C-domain) fold in parallel and complete folding of both domains is
513 kinetically indistinguishable (Pan et al., 1999; Kent et al., 2000). RNAs can be classified as
514 slow and fast folding, strongly depending on temperature and ionic conditions. The nature of
515 the rate-limiting step (from the I to the N state) for the slow-folding class can be assigned to
516 disruption of non-native or prematurely formed native structures (folding traps). By contrast,
517 the fast-folding class is thought to solely involve small-scale conformational changes, for
518 example the rearrangement of prebound metal ions (Fang et al., 2002; Sosnick and Pan,
519 2004, and refs. therein). It was shown for the mesophilic *B. subtilis* P RNA that the full-length
520 RNA belongs to the class of slow folding RNAs (~0.2 min⁻¹; measured at 20 mM Tris, pH 8.1,
521 10 to 20 mM Mg²⁺ and 37°C; Pan and Sosnick, 1997), whereas its isolated C-domain is a
522 member of the fast-folding class (390 min⁻¹; measured at 37.5°C, 20 mM Tris, pH 8.1, 10 mM
523 Mg²⁺; Fang et al., 1999). The *B. subtilis* S-domain folds at a rate of 4.5 min⁻¹ (Sosnick and

524 Pan, 2004), suggesting that slow folding of the full-length P RNA involves searches for intra-
525 and interdomain contacts during transition to the native structure. Baird et al. (2006) studied
526 the I-to-N transition of the isolated *Tth* P RNA S-domain by CD spectroscopy relative to the
527 S-domain of *Eco* P RNA. The *Tth* S-domain folded at a lower Mg^{2+} concentration with
528 increased Mg^{2+} cooperativity and increased denaturant-sensitive surface burial relative to the
529 mesophilic S-domain. Increased surface burial is in line with stronger protection of the *Tth* S-
530 domain from RNase T1 cleavage when changing from the I to the N state compared with the
531 *Eco* S-domain (Baird et al., 2006). Folding equilibria for the two S-domains were analyzed at
532 37°C in the study by Baird et al. (2006) but using an extended time window for the *Tth* S-
533 domain (up to 70 min) relative to the mesophilic counterpart (up to 9 min). This indicates that
534 already the *Tth* S-domain folds at a slower rate than the *Eco* S-domain at 37°C, but its
535 activation energy barrier for the I-to-N transition is clearly lower than for the *Tth* full-length P
536 RNA that requires a temperature \gg 37°C for efficient folding (Fig. 5). The high temperature
537 requirement for *Tth* P RNA folding and the ~fourfold acceleration of the folding rate by the
538 presence of 3 M urea (Supplemental Fig. S3) indicate that the major activation barrier along
539 the RNA folding pathway is caused by formation of non-native structures.

540 These findings are in line with results from previous folding studies of *E. coli* and *B.*
541 *subtilis* P RNAs, showing that formation of P6 and P7 is among the late events in the folding
542 pathway (Zarrinkar et al., 1996; Kent et al., 2000). Backbone discontinuity between P5 and
543 P7 in a circularly permuted *B. subtilis* P RNA (with the natural 5'- and 3'-ends connected by a
544 loop; termed cp240 RNA) enhanced folding 15-fold at 37°C, supporting the idea of a folding
545 trap involving the P7 region (Zarrinkar et al., 1996; Pan et al., 1999). *Tth* P RNA *in silico*
546 folding with RNAfold (default parameters; Lorenz et al., 2011) predicts most secondary
547 structural elements (including P5 at the domain interface) except for the pseudoknots P4 and
548 P6. However, an alternative structure in the S-domain close to the domain interface,
549 involving pairings between 5'-P6/3'-P7 and 5'-P7/3'-P10/P11, is predicted as well
550 (Supplemental Fig. S5). Such a misfold would be consistent with the reported findings cited
551 above.

552 Our probing experiments showed compactions in several regions of the *Tth* S-domain
553 upon preincubation at 55°C, prominently in 5'-P6 and 5'-P7 at the junction between the two
554 domains, but also in the C-domain in P3, J3/4 and helix P4 near its U bulge in the catalytic
555 core as inferred from changes in RNase T1 accessibility (Fig. 6). Formation of the L8-P4
556 contact might be a major factor contributing to this structural adjustment of the catalytic core.
557 We further noticed some changes in RNase T1 accessibility in the P15-17 subdomain (~ nt
558 250-295; Figs. 6A, C). This may be interpreted as suggesting that this subdomain is
559 reoriented upon formation of P6. In summary, the *Tth* P RNA belongs to a small group of
560 natural thermostable RNAs with very high G,C content, resulting in enhanced stability of its
561 secondary and tertiary structure. The RNA is assumed to fold into its active structure without
562 assistance of protein cofactors. The high G,C content and structural stability of the RNA is
563 associated with higher activation barriers that need to be surmounted for proceeding from
564 intermediate folding states to the native fold or to resolve off-pathway folding traps. Here we
565 showed that an intermediate, likely involving non-native interactions of sequences at the
566 junction of C- and S-domain, can only be resolved at temperatures as high as 55°C. Folding
567 from the intermediate to the native fold resulted in substantial structural compaction and loss
568 of surface accessibility, in line with the results of the previous study on the isolated *Tth* S-
569 domain (see above; Baird et al., 2006).

570

571 **MATERIALS & METHODS**

572

573 **UV melting**

574 UV melting profiles were recorded on a Uvikon XL UV/Vis spectrophotometer coupled to a
575 Peltier thermosystem (Biotek) and an automated cell changer for 10 cells and 2 references.
576 The temperature controller was ramped at a rate of 0.5°C / min from 10°C to 90°C, and data
577 points were collected every 0.4°C as determined by a temperature probe inserted into a
578 cuvette containing the final buffer. Samples were measured in 10 mM sodium cacodylate
579 buffer pH 7, 0.5 mM EDTA and 100 mM NaCl at an RNA concentration of 25 nM. For data

580 analysis, a script was written to convert concatenated Uvikon report text files into separate
581 denaturation and annealing segments for each position. These were subsequently subjected
582 to piece-wise linear interpolation and smoothed over a 5°C window. From this data, the first
583 derivative of absorbance curves (dA_{260}/dT versus T) were calculated and plotted as a
584 function of temperature, using either Kaleidagraph 4.0 (Synergy Software), or Xmgrace.
585 Xmgrace was also used to fit Gaussian normal distributions to derivative melting profiles.
586 Initial constraints were the number of distributions and the starting T_m , which were iteratively
587 adapted until convergence was obtained.

588

589 **Construction of plasmids encoding mutant P RNAs used as transcription templates**

590 Transcription templates for mutant P RNAs (pUC19 derivatives) were constructed using
591 standard PCR techniques as described in Li et al. (2009) or using the Stratagene
592 Quikchange site-directed mutagenesis protocol; DNA sequences were verified by dideoxy
593 sequencing (e.g. custom service by Eurofins Genomics).

594

595 ***In vitro* transcription and labeling of RNA 5' or 3' ends**

596 RNAs were produced by run-off transcription with T7 RNA polymerase and subsequent gel
597 purification as described in Busch *et al.* (2000). The substrate, *Tth* pre-tRNA^{Gly}, was
598 transcribed from plasmid pSBpt3'HH linearized with BamHI (Busch et al. 2000), *Eco* P RNA
599 from plasmid pJA2' (Vioque et al., 1988) linearized with FokI; *Tth*, *Dra* and *Ptr* WT and
600 mutant P RNAs were transcribed from the respective pUC19 derivative plasmids linearized
601 with Ehel, BbsI and FokI, respectively. 5'-endlabeling of pre-tRNA^{Gly} and 5' as well as 3'-
602 endlabeling of P RNAs were performed as detailed in Heide et al. (1999).

603

604 **Probing experiments**

605 *Partial hydrolysis of T. thermophilus P RNA by RNase T1*

606 Limited digestion by RNase T1 was performed by incubation of 3'- or 5'-endlabeled *T.*
607 *thermophilus* P RNA (20,000 Cherenkov cpm, also containing 60 ng/ μ l *A. aeolicus* 6S RNA

608 as carrier) for 10 min at 37°C or 55°C in buffer A (20 mM sodium citrate/HCl, 0.2 mM EDTA,
609 7 M urea, pH 5.0) for denaturing conditions or buffer B (50 mM Hepes pH 7.0, 4.5 mM
610 Mg(OAc)₂, 0.1 M NH₄OAc, pH 7.5 at 37°C) for native conditions. Hydrolysis was started by
611 addition of RNase T1 (Thermo Fisher Scientific) to a final concentration of 0.16 U/μl followed
612 by 10 min incubation at 37°C and ethanol precipitation to stop the reaction.

613

614 *Iodine-induced hydrolysis of phosphorothioate analogue-modified P RNA*

615 For generation of U or A ladders, modified *T. thermophilus* P RNA was used. Incorporation of
616 ATP-αS or UTP-αS nucleotides (to around 5% modification) was achieved by run-off
617 transcription (Busch et al., 2000; Heide et al., 2001) using the T7 Y639F mutant RNA
618 polymerase (Sousa et al. 1995). Iodine hydrolysis was performed in the presence of 10 mM
619 Tris-HCl pH 7.5, 60 ng/μl of *A. aeolicus* 6S RNA as carrier RNA and 0.1 mg/ml I₂ for 20 min
620 at 37°C.

621

622 *Probing gels*

623 All probing samples were loaded onto 12% PAA/8 M urea gels (thickness: 0.4 mm; width: 16
624 cm; length: 40 cm); gels were run at 6-10 mA until xylene cyanol had migrated ~ 36 cm from
625 the slot.

626

627 **Complementation analyses in the *E. coli rnpB* complementation strain BW**

628 *In vivo* complementation assays were performed in the *E. coli rnpB* mutant strain BW with
629 derivatives of plasmid pACYC177 as previously described (Wegscheid and Hartmann, 2006);
630 plasmid-borne P RNA coding sequences to be tested were embedded between the native *E.*
631 *coli rnpB* promoter and 3'-precursor/terminator region using standard PCR techniques.

632

633 **Preparation of recombinant RNase P proteins**

634 *E. coli* and *B. subtilis* RNase P proteins carrying an N-terminal His-tag (His-tagged peptide
635 leader: MRGSHHHHHHGS, encoded in plasmid pQE-30 in *E. coli* JM109) were expressed

636 and purified essentially as described (Rivera-Leon et al., 1995).

637

638 **Enzyme kinetics**

639 For single-turnover RNA-alone reactions (Table 1), trace amounts (≤ 1 nM) of 5'-³²P-
640 endlabeled *T. thermophilus* pre-tRNA^{Gly} substrate were preincubated in reaction buffer C
641 (100 mM Mg[OAc]₂, 100 mM NH₄OAc, 0.1 mM EDTA, 50 mM MES, pH 6.0 at 37°C) for 5
642 min at 55°C and 25 min at 37°C. P RNAs (varied in the range of 0.1 to 15 μM) were
643 preincubated in the same buffer for 5 min at 55°C and 55 min at 37°C. Processing reactions
644 were started by combining enzyme and substrate solutions and assayed at 37°C.

645 Multiple turnover reactions catalyzed by *Tth* P RNA were performed in buffer D (20
646 mM Mg[OAc]₂, 100 mM NH₄OAc, 50 mM HEPES, pH 7.0), using 20 nM P RNA and 200 mM
647 pre-tRNA^{Gly}, if not stated otherwise, with P RNA preincubation conditions specified in the
648 figure legend. For reaction conditions in Supplemental Figs. S2 and S3, see the respective
649 figure legends.

650 For cleavage assays with reconstituted RNase P holoenzymes, buffer KN (20 mM
651 HEPES-NaOH, 2 mM or 4.5 mM Mg[OAc]₂, 150 mM NH₄OAc, 2 mM spermidine, 0.05 mM
652 spermine, and 4 mM β-mercaptoethanol, pH 7.4) (Dinos et al. 2004) was used to closely
653 mimic physiological conditions. *In vitro* reconstitution of RNase P holoenzymes was
654 performed as follows: P RNAs were incubated in buffer KN for 5 min at 55°C and 50 min at
655 37°C, after which RNase P protein was added, followed by another 5 min at 37°C before
656 addition of substrate. Cleavage assays were performed at 37°C. Aliquots of the cleavage
657 reactions were withdrawn at various time points and analyzed by electrophoresis on 20%
658 polyacrylamide/8 M urea gels. Data analysis and calculations were performed essentially as
659 previously described (Busch et al. 2000). Briefly, gels were subjected to phosphorimaging
660 and radioactive bands representing substrate and 5'-cleavage product were quantified with
661 the AIDA (raytest) image analysis software. First-order rate constants of cleavage (k_{obs}) were
662 calculated by fitting the data to the equation for a single exponential: $f_{\text{cleaved}} = f_{\text{endpoint}} \times (1 -$

663 $e^{-(k_{obs}) \times t}$, where $f_{cleaved}$ = fraction of substrate cleaved, t = time, $f_{endpoint}$ = maximum
664 cleavable substrate (Grafit version 5.0.13, Erithacus Software). For determination of single
665 turnover V_{max} (k_{react}) and K_M ($K_{M(sto)}$) values, k_{obs} values measured at 5 different enzyme
666 concentrations (based on at least 3 replicate experiments each) were plotted against the
667 enzyme concentration; k_{react} and $K_{M(sto)}$ were obtained by fitting the data to a “Michaelis-
668 Menten-like” enzyme kinetics model: $k_{obs} = k_{react} \times [P\ RNA]/(K_{M(sto)} + [P\ RNA])$. For
669 experimental conditions in Supplemental Fig. S4, see figure legend.

670

671 **ACKNOWLEDGEMENTS**

672

673 This work was supported by the German Research Foundation (DFG), grant HA1672/19-1 to
674 RKH.

675

676 **REFERENCES**

677

- 678 Airo A, Chan SL, Martinez Z, Platt MO, Trent JD. 2004. Heat shock and cold shock in
679 *Deinococcus radiodurans*. *Cell Biochem Biophys* **40**: 277-288. doi:
680 10.1385/CBB:40:3:277
- 681 Anantharaman V, Aravind L. 2006. The NYN domains: novel predicted RNAses with a PIN
682 domain-like fold. *RNA biology* **3**:18-27. doi: 10.4161/rna.3.1.2548
- 683 Appukuttan D, Rao AS, Apte SK. 2006. Engineering of *Deinococcus radiodurans* R1 for
684 Bioprecipitation of Uranium from Dilute Nuclear Waste. *Appl Environm Microbiol* **72**:
685 7873–7878. doi: 10.1128/AEM.01362-06
- 686 Baird NJ, Srividya N, Krasilnikov AS, Mondragón A, Sosnick TR, Pan T. 2006. Structural
687 basis for altering the stability of homologous RNAs from a mesophilic and a
688 thermophilic bacterium. *RNA* **12**: 598-606. doi: 10.1261/rna.2186506
- 689 Battista JR. 1997. Against all odds: The Survival Strategies of *Deinococcus radiodurans*.
690 *Annu Rev Microbiol* **51**: 203–224. doi: 10.1146/annurev.micro.51.1.203

- 691 Brown JW. 1999. The Ribonuclease P Database. *Nucleic Acids Res* **27**: 314. doi:
692 10.1093/nar/27.1.314
- 693 Brown JW, Nolan JM, Haas ES, Rubio MA, Major F, Pace NR. 1996. Comparative analysis
694 of ribonuclease P RNA using gene sequences from natural microbial populations
695 reveals tertiary structural elements. *Proc Natl Acad Sci U S A* **93**: 3001-3006. doi:
696 10.1073/pnas.93.7.3001
- 697 Busch S, Kirsebom LA, Notbohm H, Hartmann RK. 2000. Differential role of the
698 intermolecular base-pairs G292-C(75) and G293-C(74) in the reaction catalyzed by
699 *Escherichia coli* RNase P RNA. *J Mol Biol* **299**: 941-951. doi: 10.1006/jmbi.2000.3789
- 700 Corsaro MM, Lanzetta R, Parrilli E, Parrilli M, Tutino ML, Ummarino S. 2004. Influence of
701 growth temperature on lipid and phosphate contents of surface polysaccharides from
702 the antarctic bacterium *Pseudoalteromonas haloplanktis* TAC 125. *J Bacteriol* **186**: 29-
703 34. doi: 10.1128/jb.186.1.29-34.2004
- 704 Darr SC, Zito K, Smith D, Pace NR. 1992. Contributions of phylogenetically variable
705 structural elements to the function of the ribozyme ribonuclease P. *Biochemistry* **31**:
706 328-333. doi: 10.1021/bi00117a003
- 707 Dinos G, Wilson DN, Teraoka Y, Szaflarski W, Fucini P, Kalpaxis D, Nierhaus KH. 2004.
708 Dissecting the ribosomal inhibition mechanisms of edeine and pactamycin: the
709 universally conserved residues G693 and C795 regulate P-site RNA binding. *Mol Cell*
710 **13**: 113-24. doi: 10.1016/s1097-2765(04)00002-4
- 711 Doherty EA, Batey RT, Masquida B, Doudna JA. 2001. A universal mode of helix packing in
712 RNA. *Nat Struct Biol* **8**: 339-343. doi: 10.1038/86221.
- 713 Doherty EA, Doudna JA. 1997. The P4-P6 domain directs higher order folding of the
714 *Tetrahymena* ribozyme core. *Biochemistry* **36**: 3159-3169. doi: 10.1021/bi962428+
- 715 Fang XW, Thiyagarajan P, Sosnick TR, Pan T. 2002. The rate-limiting step in the folding of a
716 large ribozyme without kinetic traps. *Proc Natl Acad Sci U S A* **99**: 8518-8523. doi:
717 10.1073/pnas.142288399

- 718 Gößringer M, Kretschmer-Kazemi Far R, Hartmann RK. 2006. Analysis of RNase P protein
719 (rnpA) expression in *Bacillus subtilis* utilizing strains with suppressible rnpA expression.
720 *J Bacteriol* **188**: 6816-6823. doi: 10.1128/JB.00756-06
- 721 Gößringer M, Schencking I, Hartmann RK. 2021. The RNase P Ribozyme. In *Ribozymes:*
722 *Principles, Methods, Applications* (eds. S Müller, B. Masquida and W. Winkler), in
723 press. Wiley-VCH, Weinheim, Germany.
- 724 Guerrier-Takada C, Gardiner K, Marsh T, Pace N, Altman S. 1983. The RNA moiety of
725 ribonuclease P is the catalytic subunit of the enzyme. *Cell* **35**: 849-857. doi:
726 10.1016/0092-8674(83)90117-4
- 727 Haas ES, Banta AB, Harris JK, Pace NR, Brown JW. 1996. Structure and evolution of
728 ribonuclease P RNA in Gram-positive bacteria. *Nucleic Acids Res* **24**: 4775-4782. doi:
729 10.1093/nar/24.23.4775
- 730 Haas ES, Brown JW, Pitulle C, Pace NR. 1994. Further perspective on the catalytic core and
731 secondary structure of ribonuclease P RNA. *Proc Natl Acad Sci U S A* **91**: 2527-2531.
732 doi: 10.1073/pnas.91.7.2527
- 733 Haas ES, Brown JW. 1998. Evolutionary variation in bacterial RNase P RNAs. *Nucleic Acids*
734 *Res* **26**: 4093-4099. doi: 10.1093/nar/26.18.4093
- 735 Hardt W-D, Hartmann RK. 1996. Mutational analysis of the joining regions flanking helix P18
736 in *E. coli* RNase P RNA. *J Mol Biol* **259**: 422-433. doi: 10.1006/jmbi.1996.0329
- 737 Hartmann RK, Gößringer M, Späth B, Fischer S, Marchfelder A. 2009. The making of tRNAs
738 and more – RNase P and tRNAse Z. *Prog Mol Biol Transl Sci* **85**: 319-368. doi:
739 10.1016/S0079-6603(08)00808-8
- 740 Heide C, Pfeiffer T, Nolan JM, Hartmann RK. 1999. Guanosine 2-NH₂ groups of *Escherichia*
741 *coli* RNase P RNA involved in intramolecular tertiary contacts and direct interactions
742 with tRNA. *RNA* **5**: 102-116. doi: 10.1017/s1355838299981499
- 743 Heide C, Feltens R, Hartmann RK. 2001. Purine N7 groups that are crucial to the interaction
744 of *Escherichia coli* RNase P RNA with tRNA. *RNA* **7**: 958-968. doi:
745 10.1017/s1355838201001753

- 746 Jarrous N, Gopalan V. 2010. Archaeal/eukaryal RNase P: subunits, functions and RNA
747 diversification. *Nucleic Acids Res* **38**: 7885-7894. doi: 10.1093/nar/gkq701
- 748 Kent O, Chaulk SG, MacMillan AM. 2000. Kinetic analysis of the M1 RNA folding pathway. *J*
749 *Mol Biol* **304**: 699-705. doi: 10.1006/jmbi.2000.4263
- 750 Klemm BP, Wun N, Chen Y, Liu X, Kaitany KJ, Howard MJ, Fierke CA. 2016. The Diversity
751 of Ribonuclease P: Protein and RNA Catalysts with Analogous Biological Functions.
752 *Biomolecules* **13**: 6. doi: 10.3390/biom6020027
- 753 Köhler K, Duchardt-Ferner E, Lechner M, Damm K, Hoch PG, Salas M, Hartmann RK. 2015.
754 Structural and mechanistic characterization of 6S RNA from the hyperthermophilic
755 bacterium *Aquifex aeolicus*. *Biochimie* **117**: 72-86. doi: 10.1016/j.biochi.2015.03.004
- 756 Lai LB, Tanimoto A, Lai SM, Chen WY, Marathe IA, Westhof E, Wysocki VH, Gopalan V.
757 2017. A novel double kink-turn module in euryarchaeal RNase P RNAs. *Nucleic Acids*
758 *Res* **45**: 7432-7440. doi: 10.1093/nar/gkx388
- 759 Li D, Willkomm DK, Hartmann RK. 2009. Minor changes largely restore catalytic activity of
760 archaeal RNase P RNA from *Methanothermobacter thermoautotrophicus*. *Nucleic*
761 *Acids Research* **37**: 231–242. doi: 10.1093/nar/gkn915
- 762 Loria A, Pan T. 1996. Domain structure of the ribozyme from eubacterial ribonuclease P.
763 *RNA* **2**: 551–563.
- 764 Lorenz R, Bernhart SH, Hoener zu Siederdisen C, Tafer H, Flamm C, Stadler PF, Hofacker
765 IL (2011). ViennaRNA Package 2.0. *Algorithms for Molecular Biology* **6**:26.
- 766 Mao G, Srivastava AS, Wu S, Kosek D, Lindell M, Kirsebom LA. 2018. Critical domain
767 interactions for type A RNase P RNA catalysis with and without the specificity domain.
768 *PLoS One* **13**: e0192873. doi: 10.1371/journal.pone.0192873.
- 769 Marszalkowski M, Teune JH, Steger G, Hartmann RK, Willkomm DK. 2006. Thermostable
770 RNase P RNAs lacking P18 identified in the Aquificales. *RNA* **12**: 1915-1921. doi:
771 10.1261/rna.242806

- 772 Marszalkowski M, Willkomm DK, Hartmann RK. 2008. Structural basis of a ribozyme's
773 thermostability: P1-L9 interdomain interaction in RNase P RNA. *RNA* **14**: 127-133. doi:
774 10.1261/rna.762508
- 775 Massire C, Jaeger L, Westhof E. 1997. Phylogenetic evidence for a new tertiary interaction in
776 bacterial RNase P RNAs. *RNA* **3**: 553-556.
- 777 Massire C, Jaeger L, Westhof E. 1998. Derivation of the three-dimensional architecture of
778 bacterial ribonuclease P RNAs from comparative sequence analysis. *J Mol Biol*, **279**:
779 773-793. doi: 10.1006/jmbi.1998.1797
- 780 Matelska D, Steczkiewicz K, Ginalski K. 2017. Comprehensive classification of the PIN
781 domain-like superfamily. *Nucleic Acids Res.* **45**: 6995–7020. doi: 10.1093/nar/gkx494
- 782 Medigue C, Krin E, Pascal G, Barbe V, Bernsel A, Bertin PN, Cheung F, Cruveiller S,
783 D'Amico S, Duilio A., et al. 2005. Coping with cold: the genome of the versatile marine
784 Antarctica bacterium *Pseudoalteromonas haloplanktis* TAC125. *Genome Res* **15**:
785 1325-1335. doi: 10.1101/gr.4126905
- 786 Nickel AI, Wäber NB, Gößringer M, Lechner M, Linne U, Toth U, Rossmann W, Hartmann
787 RK. 2017. Minimal and RNA-free RNase P in *Aquifex aeolicus*. *Proc Natl Acad Sci U S*
788 *A* **114**: 11121-11126. doi: 10.1073/pnas.1707862114
- 789 Ohima T, Imahori K. 1974. Description of *Thermus thermophilus* (Yoshida and Ohima)
790 comb. nov., a Nonsporulating Thermophilic Bacterium from a Japanese Thermal Spa.
791 *Int J Systemat Bacteriol* **24**: 102-112.
- 792 Pan T, Fang X, Sosnick T. 1999. Pathway Modulation, Circular Permutation and Rapid RNA
793 Folding Under Kinetic Control. *J Mol Biol* **286**: 721-731. doi: 10.1006/jmbi.1998.2516
- 794 Pan T, Sosnick T. 1997. Intermediates and kinetic traps in the folding of a large ribozyme
795 revealed by circular dichroism and UV absorbance spectroscopies and catalytic
796 activity. *Nat Struct Biol* **4**: 931-938. doi: 10.1038/nsb1197-931
- 797 Pomeranz Krummel DA, Altman S. 1999. Verification of phylogenetic predictions in vivo and
798 the importance of the tetraloop motif in a catalytic RNA. *Proc Natl Acad Sci U S A* **96**:
799 11200-11205. doi: 10.1073/pnas.96.20.11200.

- 800 Reiter NJ, Osterman A, Torres-Larios A, Swinger KK, Pan T, Mondragón A. 2010 Structure
801 of a bacterial ribonuclease P holoenzyme in complex with tRNA. *Nature* **468**: 784-789.
802 doi: 10.1038/nature09516
- 803 Rivera-León R, Green CJ, Vold BS. 1995. High-level expression of soluble recombinant
804 RNase P protein from *Escherichia coli*. *J Bacteriol* **177**: 2564-2566. doi:
805 10.1128/jb.177.9.2564-2566.1995
- 806 Schencking I, Rossmanith W, Hartmann RK. 2020. Diversity and Evolution of RNase P.
807 In: Pontarotti P. (eds) *Evolutionary Biology—A Transdisciplinary Approach*.
808 Springer, Cham. https://doi.org/10.1007/978-3-030-57246-4_11.
- 809 Schlegl J, Hardt WD, Erdmann VA, Hartmann RK. 1994. Contribution of structural elements
810 to *Thermus thermophilus* ribonuclease P RNA function. *EMBO J* **13**: 4863-4869.
- 811 Setlow JK, Boling ME. 1965. The resistance of *Micrococcus radiodurans* to ultraviolet
812 radiation. II. Action spectra for killing, delay in DNA synthesis, and thymine
813 dimerization. *Biochim Biophys Acta* **108**: 259–265. doi: 10.1016/0005-2787(65)90010-9
- 814 Siegel RW, Banta AB, Haas ES, Brown JW, Pace NR. 1996. *Mycoplasma fermentans*
815 simplifies our view of the catalytic core of ribonuclease P RNA. *RNA*, **2**: 452-462.
- 816 Sosnick TR, Pan T. 2004. Reduced contact order and RNA folding rates. *J Mol Biol* **342**:
817 1359-1365. doi: 10.1016/j.jmb.2004.08.002
- 818 Sousa R, Padilla R. 1995. A mutant T7 RNA polymerase as a DNA polymerase. *EMBO J* **14**:
819 4609-4621.
- 820 Vioque A, Arnez J, Altman S. 1988. Protein-RNA interactions in the RNase P holoenzyme
821 from *Escherichia coli*. *J Mol Biol* **202**: 835-848. doi: 10.1016/0022-2836(88)90562-1
- 822 Wegscheid B, Hartmann RK. 2006. The precursor tRNA 3'-CCA interaction with *Escherichia*
823 *coli* RNase P RNA is essential for catalysis by RNase P in vivo. *RNA* **12**: 2135-2148.
824 doi: 10.1261/rna.188306
- 825 Wan F, Wang Q, Tan J, Tan M, Chen J, Shi S, Lan P, Wu J, Lei M. 2019. Cryo-electron
826 microscopy structure of an archaeal ribonuclease P holoenzyme. *Nat Commun* **10**:
827 2617. doi: 10.1038/s41467-019-10496-3

- 828 Waugh DS, Green CJ, Pace NR. 1989. The design and catalytic properties of a simplified
829 ribonuclease P RNA. *Science* **244**: 1569-1571. doi: 10.1126/science.2472671
- 830 Waugh DS, Pace NR. 1990. Complementation of an RNase P RNA (rnpB) gene deletion in
831 *Escherichia coli* by homologous genes from distantly related eubacteria. *J Bacteriol*
832 **172**: 6316-6322. doi: 10.1128/jb.172.11.6316-6322.1990
- 833 Wegscheid B, Hartmann RK. 2006. The precursor tRNA 3'-CCA interaction with *Escherichia*
834 *coli* RNase P RNA is essential for catalysis by RNase P in vivo. *RNA* **12**: 2135-2148.
835 doi: 10.1261/rna.188306
- 836 Wegscheid B, Hartmann RK. 2007. In vivo and in vitro investigation of bacterial type B
837 RNase P interaction with tRNA 3'-CCA. *Nucleic Acids Res* **35**: 2060-2073. doi:
838 10.1093/nar/gkm005
- 839 Xin Y, Laing C, Leontis NB, Schlick T. 2008. Annotation of tertiary interactions in RNA
840 structures reveals variations and correlations. *RNA* **14**: 2465-2477. doi:
841 10.1261/rna.1249208

842 **TABLES**

843

844 **Table 1:** Summary of kinetic data of RNA-alone activity assays at 37°C.

	$K_{m(sto)}$ [μM]	k_{react} [min^{-1}]	$k_{react}/K_{m(sto)}$ [$\text{min}^{-1} \mu\text{M}^{-1}$]	$k_{react}/K_m (WT) /$ $k_{react}/K_m (mut)$
<i>Eco</i> WT	0.65 (± 0.02)	14.2 (± 0.1)	~22	-
<i>Eco</i> mL9	0.33 (± 0.08)	11.1 (± 0.8)	~34	~0.65
<i>Tth</i> WT	0.5 (± 0.1)	5.3 (± 0.3)	~11	-
<i>Tth</i> mL8	0.4 (± 0.1)	3.1 (± 0.1)	~8	~1.4
<i>Tth</i> mL18	1.8 (± 0.4)	3.6 (± 0.4)	~2	~5.5
<i>Tth</i> mL8/L18	1.9 (± 0.1)	1.0 (± 0.0)	~0.5	~22
<i>Tth</i> mL9	0.9 (± 0.2)	6.2 (± 0.5)	~7	~1.6
<i>Ptr</i> WT	0.4 (± 0.1)	10.5 (± 0.8)	~26	-
<i>Ptr</i> mL8	34 (± 4) $\times 10^{-2}$	23 (± 1) $\times 10^{-2}$	~0.7	~37
<i>Ptr</i> mL18	29 (± 2) $\times 10^{-2}$	21 (± 1) $\times 10^{-2}$	~0.7	~37
<i>Ptr</i> mL8/L18	0.4 (± 0.1)	2.2 (± 0.2) $\times 10^{-2}$	~0.06	~430
<i>Ptr</i> mL9	46 (± 6) $\times 10^{-2}$	11.0 (± 0.5)	~24	~1.1
<i>Dra</i> WT	0.8 (± 0.1)	4.4 (± 0.3)	~5.5	-
<i>Dra</i> mP9c	0.9 (± 0.2)	0.7 (± 0.1)	~0.8	~6.9
<i>Dra</i> mL8	7.0 (± 1.7)	0.4 (± 0.1)	~0.06	~92
<i>Dra</i> mL9	1.1 (± 0.2)	4.4 (± 0.3)	~4	~1.4
<i>Dra</i> mL18	2.0 (± 0.5)	0.4 (± 0.0)	~0.2	~28
<i>Dra</i> mL8/L18	16.3 (± 5.2)	2.8 (± 0.5) $\times 10^{-2}$	~2 $\times 10^{-3}$	~3000

845 WT: wild type; $K_{m(sto)}$: single turnover K_m ; k_{react} : single turnover V_{max} . All quantifications are
846 based on at least three independent experiments; errors are standard errors of the curve fit;
847 assay conditions: 100 mM Mg(OAc)₂, 100 mM NH₄OAc, 0.1 mM EDTA, 50 mM MES, pH
848 6.0, trace amounts (< 1 nM) of *T. thermophilus* ptRNA^{Gly}, excess amounts of P RNA (E>>S);
849 preincubations: P RNA, 5 min at 55°C and 55 min at 37°C; substrate: 5 min at 55°C and 25
850 min at 37°C. Data for *Eco* P RNA shown for comparison are taken from Marszalkowski et al.
851 (2008).

852

853

854

855

856 **Table 2:** Holoenzyme kinetics for *P. translucida*, *T. thermophilus* and *D. radiodurans* P
 857 RNAs and mL9 variants thereof reconstituted with the *E. coli* or *B. subtilis* P protein.

P (RNA)	$k_{\text{obs}}(\text{min}^{-1})$	
	<i>E. coli</i> P protein	<i>B. subtilis</i> P protein
<i>Eco</i> WT 2 mM Mg ²⁺	3.8 (± 0.4)	3.0 (± 0.3)
<i>Eco</i> WT 4.5 mM Mg ²⁺	3.8 (± 0.4)	4.0 (± 0.3)
<i>Ptr</i> WT 2 mM Mg ²⁺	3.2 (± 0.1)	4.2 (± 0.04)
<i>Ptr</i> WT 4.5 mM Mg ²⁺	3.1 (± 0.2)	3.0 (± 0.2)
<i>Ptr</i> mL9 2 mM Mg ²⁺	3.6 (± 0.5)	4.7 (± 0.1)
<i>Ptr</i> mL9 4.5 mM Mg ²⁺	3.8 (± 0.5)	3.8 (± 0.1)
k_{obs} WT / k_{obs} mL9	~0.9 (2 mM Mg ²⁺) ~0.8 (4.5 mM Mg ²⁺)	~0.9 (2 mM Mg ²⁺) ~0.8 (4.5 mM Mg ²⁺)
<i>Tth</i> WT 2 mM Mg ²⁺	1.3 (± 0.2)	1.1 (± 0.1)
<i>Tth</i> WT 4.5 mM Mg ²⁺	4.0 (± 0.4)	3.5 (± 0.4)
<i>Tth</i> mL9 2 mM Mg ²⁺	5.4 (± 0.8) × 10 ⁻²	0.28 (± 0.03)
<i>Tth</i> mL9 4.5 mM Mg ²⁺	0.2 (± 0.02)	0.55 (± 0.02)
k_{obs} WT / k_{obs} mL9	24.1 (2 mM Mg ²⁺) 20 (4.5 mM Mg ²⁺)	3.9 (2 mM Mg ²⁺) 6.4 (4.5 mM Mg ²⁺)
<i>Dra</i> WT 2 mM Mg ²⁺	1.8 (± 0.6)	4.0 (± 1.2)
<i>Dra</i> WT 4.5 mM Mg ²⁺	8.7 (± 2.3)	6.7 (± 2.9)
<i>Dra</i> mL9 2 mM Mg ²⁺	1.2 (± 0.1)	0.6 (± 0.2)
<i>Dra</i> mL9 4.5 mM Mg ²⁺	7.4 (± 3.1)	7.0 (± 1.9)
<i>Dra</i> mP9c 2 mM Mg ²⁺	≤ 10 ⁻⁴ min ⁻¹	≤ 5 × 10 ⁻⁴ min ⁻¹
<i>Dra</i> mP9c 4.5 mM Mg ²⁺	(1.7 ± 0.3) × 10 ⁻³ min ⁻¹	≤ 4 × 10 ⁻³ min ⁻¹
k_{obs} WT / k_{obs} mL9	1.5 (for 2 mM Mg ²⁺) 1.2 (for 4.5 mM Mg ²⁺)	6.4 (for 2 mM Mg ²⁺) ~1 (for 4.5 mM Mg ²⁺)
k_{obs} WT / k_{obs} mP9c	≥ 17600 (for 2 mM Mg ²⁺) 5135 (for 4.5 mM Mg ²⁺)	≥ 7900 (for 2 mM Mg ²⁺) 1680 (for 4.5 mM Mg ²⁺)

858 Reactions were performed as multiple turnover kinetics with recombinant P protein at 37°C in
 859 buffer KN containing 20 mM Hepes, 150 mM NH₄OAc, 2 mM spermidine, 0.05 mM spermine,
 860 4 mM β-mercaptoethanol, pH 7.4 at 37°C, and 2 or 4.5 mM Mg(OAc)₂ as indicated, at
 861 concentrations of 10 nM P RNA, 100 nM substrate and 40 nM P protein; k_{obs} is given as

862 nmoles substrate converted per nmole of RNase P RNA per min. The data for *Eco* and *Tth* P
 863 RNA shown for comparison are taken from Marszalkowski et al. (2008).

864

865

866

867

868

869 **Table 3:** *In vivo* complementation screen in *E. coli mpB* mutant strain BW

<i>mpB</i>	37°C	43°C
<i>Eco</i> WT	++	++
<i>Eco</i> mL9	++	++
<i>Ptr</i> WT	++	++
<i>Ptr</i> mL8	-	-
<i>Ptr</i> mL18	+	+
<i>Ptr</i> mL8/L18	-	-
<i>Ptr</i> mL9	++	++
<i>Tth</i> WT	-	-
<i>Dra</i> WT	-	-

870 Growth of cells was monitored in the presence of 0.5% (w/v) glucose (without arabinose),
 871 conditions under which the chromosomal *mpB* gene of the *E. coli* mutant strain BW is not
 872 expressed (at 37° as well as 43°C); cells were transformed with derivatives of the low copy
 873 plasmid pACYC177 that contained *mpB* genes coding for P RNAs and mutants thereof under
 874 control of the native *mpB* promoter; - : no cell growth; ++ : growth with equal numbers of
 875 colonies on arabinose and glucose plates; + : somewhat decreased complementation
 876 efficiency according to number and size of colonies; WT, wild type.

877 **FIGURE LEGENDS**

878

879 **Fig. 1:** Secondary structure presentation of (A) *P. translucida* (strain TAC125), (B) *D.*
880 *radiodurans* (strain R1 dM1) and (C) *T. thermophilus* (strain HB8) P RNAs according to
881 Massire *et al.* (1998), with the three interdomain tetraloop-helix contacts L18-P8, L8-P4 and
882 L9-P1 indicated by dashed blue lines and the involved structural elements in color.
883 Nucleotide exchanges in L8, L9 and L18 (mL8, mL9 and mL18) that disrupt these tertiary
884 interactions are highlighted in red. In the *Dra* P RNA, the mP9c and 'P9c_restored' mutations
885 are illustrated in the boxes. In the *P. translucida* P RNA (panel A), the second bp in P1 is
886 shown in small letters to indicate that the bp was mutated from A:U to G:C (for details, see
887 text). Numbering in panel C is according to Schlegl *et al.* (1994); numberings in panels A and
888 B are based on the *rnpB* genes annotated in the *P. translucida* strain TAC125 chromosome I
889 (GenBank CR954246.1) and the *D. radiodurans* strain R1 dM1 chromosome I (GenBank
890 CP031500.1), respectively.

891

892 **Fig. 2:** UV absorbance (left) and derivative (right) melting profiles for *Ptr* (A), *Dra* (B), *Tth* (C)
893 P RNAs and mutants thereof, measured in 10 mM sodium cacodylate pH 7.0, 0.5 mM EDTA,
894 and 100 mM NaCl (RNA concentration 25 nM, averages of 3 to 4 curves each). Changes in
895 the melting transitions between wild type (WT) and corresponding mutant P RNAs are
896 indicated by vertical arrows in the first derivative plots on the right.

897

898 **Fig. 3:** UV absorbance (left) and derivative (right) melting profiles of the *Ptr* P RNA S-domain
899 (brown) compared to the full-length WT (green) and mL8/L18 mutant *Ptr* P RNA (blue).
900 Assay conditions were the same as in Fig. 2.

901

902 **Fig. 4:** UV absorbance (left) and derivative (right) melting profiles of *Dra* WT P RNA, the
903 mP9c and the 'P9c_restored' variant thereof (Fig. 1). For assay conditions, see legend to Fig.
904 2.

905

906 **Fig. 5:** Multiple turnover kinetics of ptRNA^{Gly} (200 nM) cleavage by *T. thermophilus* P RNA
907 (20 nM) at 20 mM Mg(OAc)₂, 100 mM NH₄OAc, 50 mM Hepes, pH 7.0 were conducted at
908 37°C, but using different preincubation procedures. Curve **a**: preincubation of P RNA for 15
909 min at 37°C before substrate addition. Curve **b**: preincubation of P RNA for 15 min at 55°C
910 before substrate addition. Curve **c**: preincubation of P RNA for 5 h at 37°C before substrate
911 addition. Curve **d**: preincubation of P RNA for 15 min at 37°C; after addition of substrate, the
912 reaction was further preincubated for 285 min (4.75 h; without withdrawal of aliquots),

913 whereupon fresh substrate (200 nM) was added (final pre-tRNA plus mature tRNA
914 concentration: 400 nM) and the processing reaction monitored for another period of 285 min.

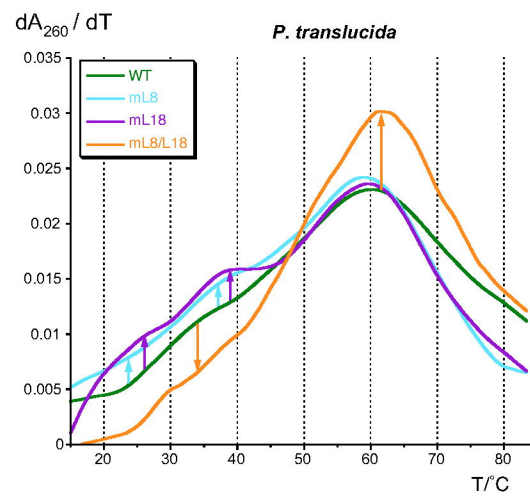
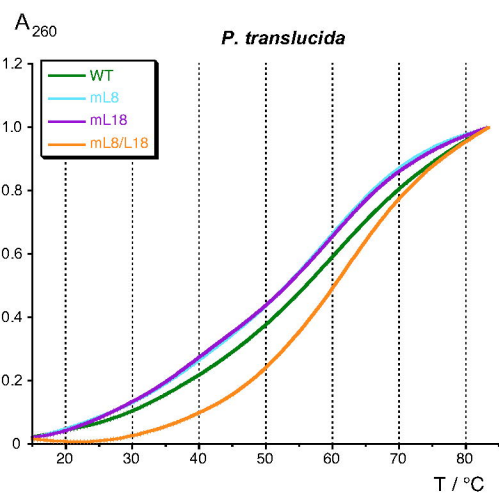
915

916 **Fig. 6:** RNase T1 probing of 5'-endlabeled *T. thermophilus* wild-type (wt) **(A)** and mL9
917 mutant P RNA **(B)**, and 3'-endlabeled wt P RNA **(C)**. Lanes A and U: AMP α S- or UMP α S-
918 substituted *T. thermophilus* wt P RNA used to generate A- and U-specific ladders by iodine
919 hydrolysis; lanes "Native 37°C" and "Native 55°C": P RNA preincubated for 10 min at 37°C or
920 55°C in the non-denaturing buffer B before addition of RNase T1 and limited hydrolysis for 10
921 min at 37°C; lanes "Denat. 37°C" and "Denat. 55°C": P RNA preincubated for 10 min at 37°C
922 or 55°C in the denaturing buffer A before addition of RNase T1 and limited hydrolysis for 10
923 min at 37°C; lanes "Con. native" and "Con. denat.": P RNA preincubated for 10 min at 55°C
924 in buffer B or buffer A, respectively, followed by incubation 10 min at 37°C without RNase
925 T1. Cleavage fragments generated by iodine hydrolysis (lanes A and U) are assigned at the
926 left (panel A) and right (panel C) margins according to the *T. thermophilus* P RNA numbering
927 system shown in Fig. 1; note that shorter fragments of A and U ladders in panel C show
928 double bands, which we attribute to end heterogeneity of the 3'-enlabeled P RNA. In panels
929 A and C, regions of *T. thermophilus* P RNA that showed reduced or enhanced RNase T1
930 accessibility after preincubation at 55°C versus 37°C are marked by gray lettering as well as
931 open and filled circles, respectively, or gray vertical lines; in panel C, structural elements are
932 given in parentheses on the left below the indicated G residues; J17/16: junction between
933 P17 and P16. Differences in the RNase T1 protection pattern between *T. thermophilus* wt
934 and mL9 P RNA are marked by vertical gray-dotted lines in panel B. The following regions
935 became protected from RNase T1 cleavage upon preincubation of 5'-endlabeled *Tth* P RNA
936 at 55°C versus 37°C (panel A): P11 (3'-strand, G226/227), L13 (G192), J11/12
937 (G127/129//132/134), P10 (114/5, weakly), P9 (G101-104), P6-8 (G74-76; G79-81;
938 G87/88/G93), P4 (G60), J3/4 (G55/56), and the 3'-side of P3 (G49/50/51/53). 3'-endlabeled
939 *Tth* P RNA (panel C) provided partially overlapping information, such as protection at G226/7
940 or signal enhancement (filled dots) at G252/3 upon preincubation at 55°C; signal intensities
941 were also increased for cleavages in the 3'-part of L15 (G291-3) and in J17/16 (G281/3).

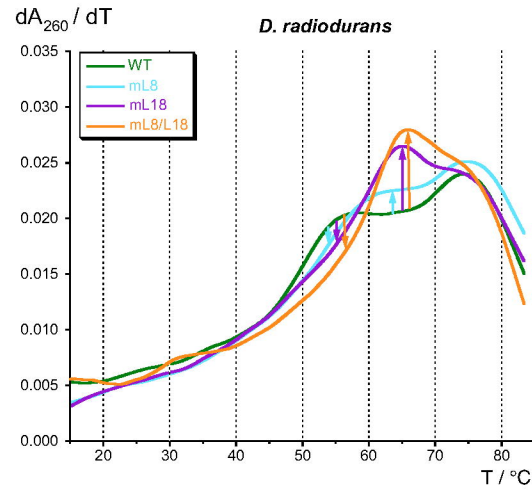
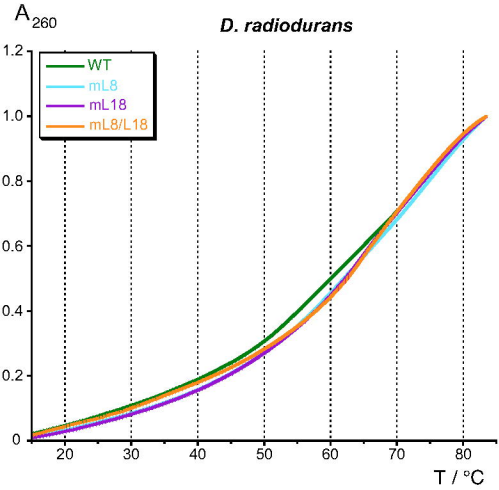
942

943 **Fig. 7:** Schematic model to explain the changes in the P RNA melting profiles (example *Tth*
944 P RNA) upon elimination of the L18-P8 and L8-P4 tertiary contacts relative to the wild-type
945 (WT) P RNA.

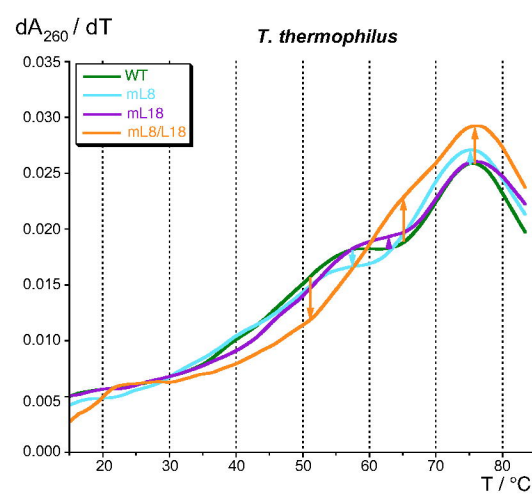
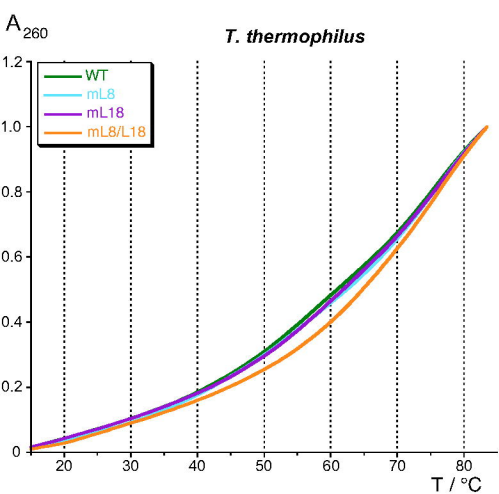
A

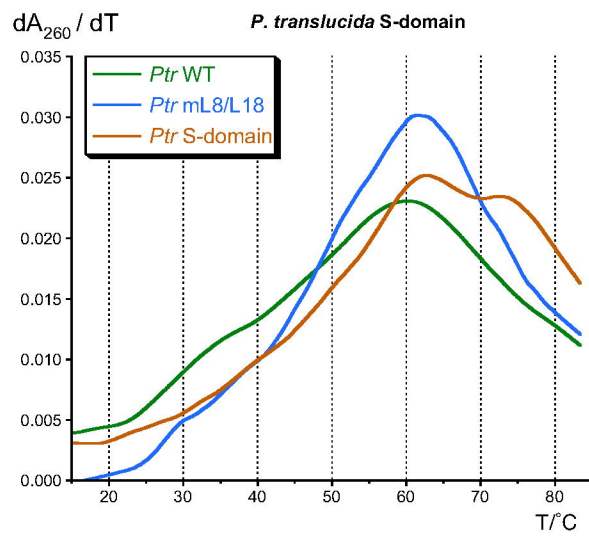
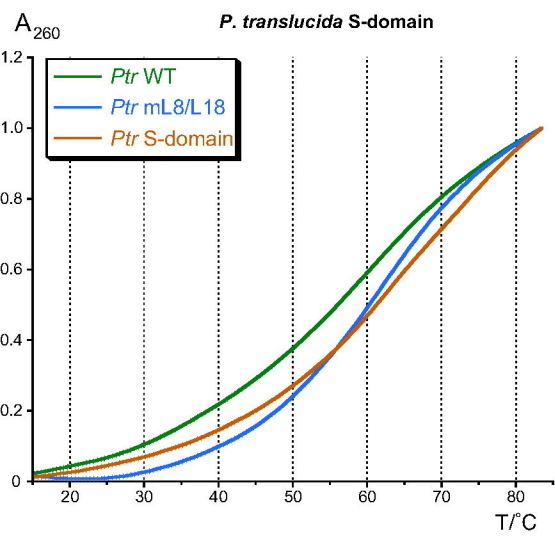


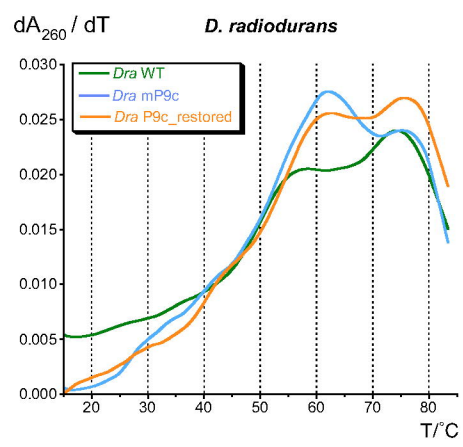
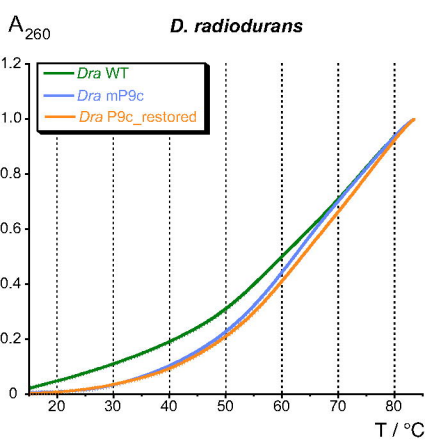
B

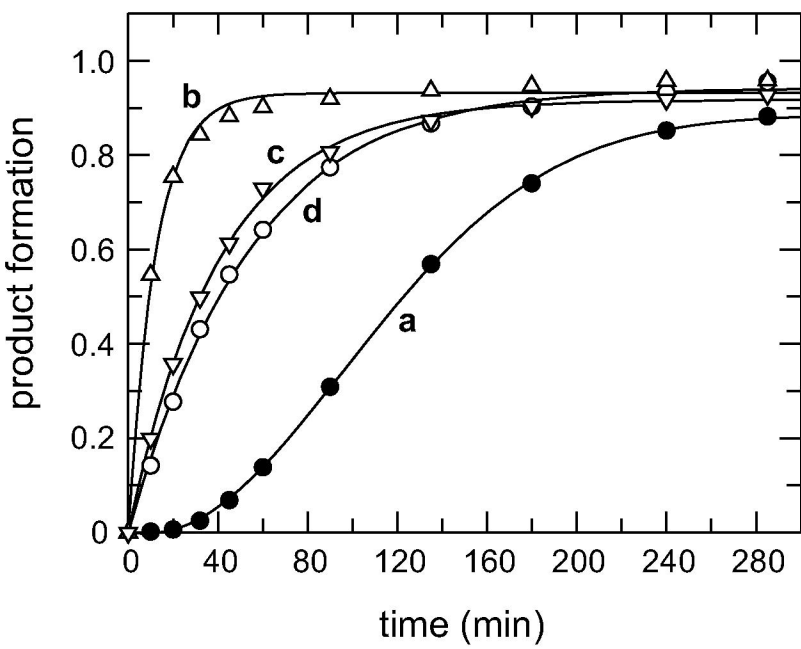


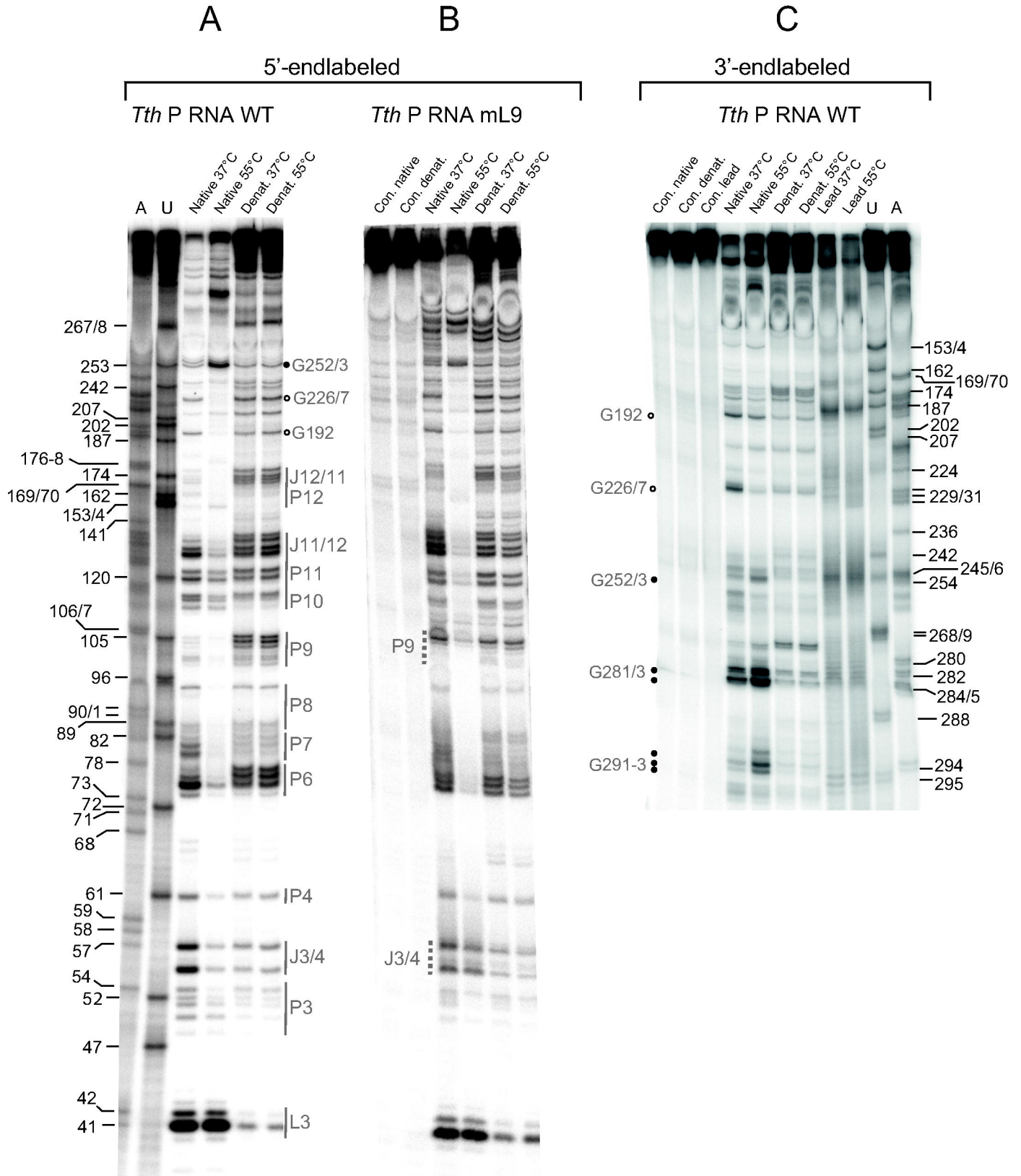
C

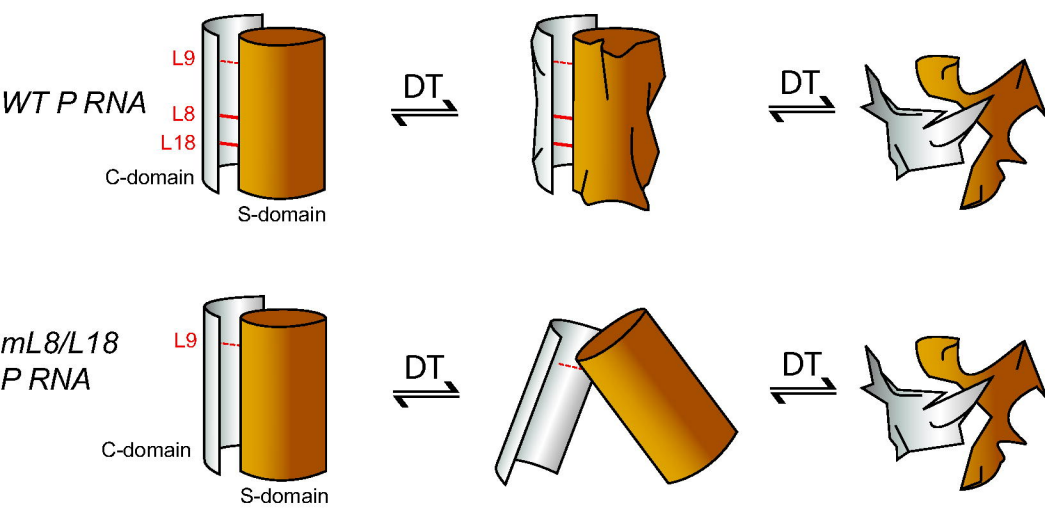














RNA

A PUBLICATION OF THE RNA SOCIETY

Comparative study on tertiary contacts and folding of RNase P RNAs from a psychrophilic, a mesophilic/radiation-resistant and a thermophilic bacterium

Michal Marszalkowski, Andreas Werner, Ralph Feltens, et al.

RNA published online July 15, 2021

Supplemental Material <http://rnajournal.cshlp.org/content/suppl/2021/07/15/rna.078735.121.DC1>

P<P Published online July 15, 2021 in advance of the print journal.

Accepted Manuscript Peer-reviewed and accepted for publication but not copyedited or typeset; accepted manuscript is likely to differ from the final, published version.

Open Access Freely available online through the *RNA* Open Access option.

Creative Commons License This article, published in *RNA*, is available under a Creative Commons License (Attribution-NonCommercial 4.0 International), as described at <http://creativecommons.org/licenses/by-nc/4.0/>.

Email Alerting Service Receive free email alerts when new articles cite this article - sign up in the box at the top right corner of the article or [click here](#).

horizon[™]
INSPIRED CELL SOLUTIONS

CRISPR knockout in iPSCs
Download our newest app note to learn how

[Download](#)

To subscribe to *RNA* go to:
<http://rnajournal.cshlp.org/subscriptions>